Journal of Advanced Joining Processes 10 (2024) 100251

Contents lists available at ScienceDirect

Journal of Advanced Joining Processes

journal homepage: www.sciencedirect.com/journal/journal-of-advanced-joining-processes

An energetic approach to the statistical analysis and optimization of friction welding processes applied to an aluminum-steel-joint

M. Winkler [a,*], C. Rößler [b], N. Harriehausen [b], S. Jüttner [c], D. Schmicker [b], F. Trommer [a]

[a] University of Applied Science Magdeburg-Stendal, Germany
[b] Sampro GmbH, Germany
[c] Otto-von-Guericke-University Magdeburg, Germany

ARTICLE INFO

Keywords:
Friction welding
Aluminum
Steel
Power
Energy
Statistical design of experiments (DoE)
Process analysis
Process optimization
Hybrid joining
Process simulation

ABSTRACT

The present publication deals with an energy-oriented approach to the statistical analysis of rotational friction welding processes. To illustrate the methodological approach, it is applied to investigate the effects of energy flow on material flow behavior and joint quality during friction welding of an AA6060 alloy with a low-alloy 16MnCr5 filler steel. The influences of the setting parameters on the energetic states are first analyzed by means of an initial screening. The evaluation using process simulation and statistical methods enables the generation of regressive response surfaces for the friction power, the friction time and the resulting induced friction energy. Based on these findings, a second experimental field is formed and evaluated, which considers the interaction between the energy input of the frictioning stage and the workpiece forging. This new approach results in the functional separation of the frictioning and forging stage, which eliminates the usual statistical interaction effects and thus facilitates analysis and optimization. The qualitative result variable required for the purpose of interpreting the results is the ultimate tensile strength of the friction-welded joint. Additionally determined hardness curves provide information about the properties of the thermally influenced zone and strength-relevant process sequences. The result is that, in addition to the amount of energy induced, the frictional power with which the former is induced also has a considerable influence on the joint strength, as it influences the material flow and the properties of the joining zone.

Introduction

In the course of current political, economic and social developments, the concept of material economy is increasingly coming to the fore in the areas of component design and production. This term includes all means and methods that serve to optimize the properties of a design with regard to economic and/or functional aspects through maximum material utilization. Essentially, an efficient use of materials results from a maximally effective interaction between the geometric component design, the material used and an optimized manufacturing process. In line with this model, there is a large and growing demand within industry for the targeted use of application-specific materials (Wang et al., 2018; Cheepu and Che, 2019; Sun et al., 2019; Fan et al., 2015) and hybrid components made of them (Wan and Huang, 2018). Such components combine different materials in a composite part and thus enable its material-based adaptation to local stresses [cf. (Draugelates et al., 2000)].

One of the most economical and productive processes for generating homogeneous and material-combining, material-locking joints is friction welding (Uday et al., 2010) acc.to Fuhaid et al. (2020), Fan et al. (2016). Due to the predominant interactions between the different materials, multimaterial systems pose particular challenges to the joining process (Winkler et al., 2023a). Specifically, these consist of limiting the formation of brittle intermetallic compounds and controlling the forced asymmetrical heat conduction (Li et al., 2014; Winiczenko et al., 2017).

This publication presents an innovative, energy-related approach for the analysis and optimization of friction welding processes, which eliminates the existing interaction effects between the frictioning and the forging stage and therefore contributes to a higher informative value of the generated results. This is exemplified by the investigation of a friction welding process to produce an aluminum-steel joint and illustrated holistically in Fig. 1.

By applying the methodology, process understanding can be

* Corresponding author.
E-mail address: marian.winkler@h2.de (M. Winkler).

https://doi.org/10.1016/j.jajp.2024.100251

Available online 4 September 2024

strengthened, as the analysis results obtained correspond to the theoretical manufacturing model. Among other things, this simplifies the transfer to SPC applications, as deviations of individual parameters in the frictioning stage can be monitored or corrected more efficiently by adjusting other friction or forging stage parameters.

State of the art

The results of previous research activities continually confirm that friction welding meets the special requirements of hybrid material combinations (Uday et al., 2010) acc.to Fuhaid et al. (2020), Fan et al. (2016). The main reason for this is the absence of material liquefaction, which eliminates many fusion welding-specific problems [cf. (Trommer, 2011)]. Since the heat input can be precisely dosed and controlled and can be adapted to the respective material, friction welding can generally be used to join more materials and material combinations than most other welding processes (Trommer, 2011).

Although a large number of materials are in principal suitable for friction welding, no statement can be made regarding the friction weldability of certain materials and workpieces on the basis of the pure material characteristics, because the tendency to form a joint is defined by a complex system consisting of the friction welding machine, clamping situation, workpiece and the friction welding process per se [cf. (Trommer, 2011)]. With regard to suitable setting parameter windows, the currently valid body of standards only provides concrete information for friction welding of some metal joints of the same type (German Welding Society (DVS), 2011). For hybrid material combinations, a statement is only made with regard to general feasibility (German Welding Society (DVS), 2009). Consequently, experimental activities are always required to determine the numerous influencing factors present and to optimally design the process-shaping setting parameters (Ostermann, 2015; Prokopczuk, 2011), cf. (Ashfaqa et al., 2011).

In order to limit the experimental effort, investigations of friction welding processes carried out in accordance with Alves et al. (2010) are limited as standard to the following essential setting parameters [as these determine the energy flow according to Seli et al. (2010) and [thus] have the greatest effect on the process according to Paventhan et al. (2012):

- the rotational friction speed (n_{rot})
- the friction pressure (p_{fric})
- the friction distance / friction time (s_{fric}/t_{fric})
- the forge pressure (p_{forge})
- the forge time (t_{forge})

Fig. 2 shows the frequency with which these setting variables were examined in the evaluated sources (Winkler et al., 2023a, 2022; Paventhan et al., 2012; Adalarasan et al., 2014; Adin et al., 2022; Ajith et al., 2015; Anand et al., 2015a, 2015b; Ananthapadmanaban et al., 2009; Asif et al., 2016; Bakkiyaraj et al., 2022; Balalan et al., 2015; Fuji, 2004; Ihsan et al., 2013; Khalfallah et al., 2020; Kumar and Ramakrishnan, 2020; Pachal and Bagesar, 2013; Paventhan et al., 2011, 2023; Rafi et al., 2010; Rajamani et al., 1992; Rangasamy et al., 2023; Sahin, 2009; Sathiya et al., 2004, 2009, 2006a, 2006b; Satyanarayana et al., 2005; Selvamani et al., 2015; Selvaraj et al., 2023; Shanjeevi et al., 2016; Sreenivasan et al., 2019; Stalin et al., 2020; Uzkut et al., 2011; Varjenju et al., 2016).

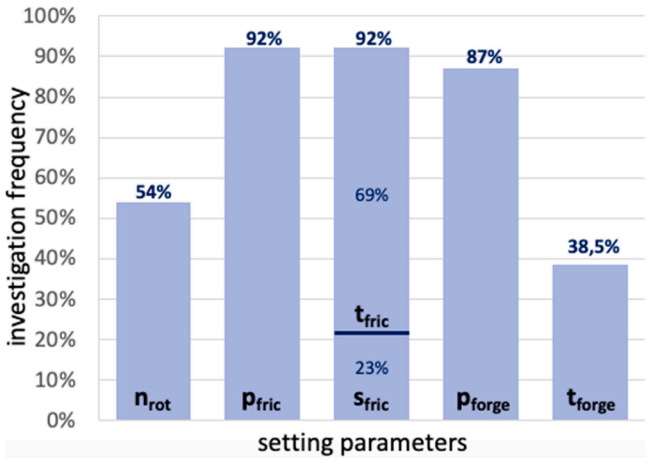

Fig. 2. Frequencies of considered setting variables in evaluated sources for the optimization of friction welding processes.

It becomes clear that in the course of documented research activities, the pressure conditions and the frictioning stage duration are predominantly considered. In the case of distance-controlled processes, the latter is characterized, among other things, by the frictional pressure, which influences the intensity of the frictional torque (M_{fric}) according to (1).

$$M_{fric} = \int \tau r \, dA = \int \mu p_{fric} r \, dA \tag{1}$$

(Trommer, 2011; Seli et al., 2010; Rößler, 2023; Kes, 1989)

Multiplied with the angular velocity (ω), this generates a friction power (P_{fric}) (2), which, depending on the friction time (t_{fric}), induces a certain amount of friction energy (En_{fric}) (3) into the system, depending on the duration of exposure. The angular velocity itself depends absolutely on the rotational friction speed (n_{rot}).

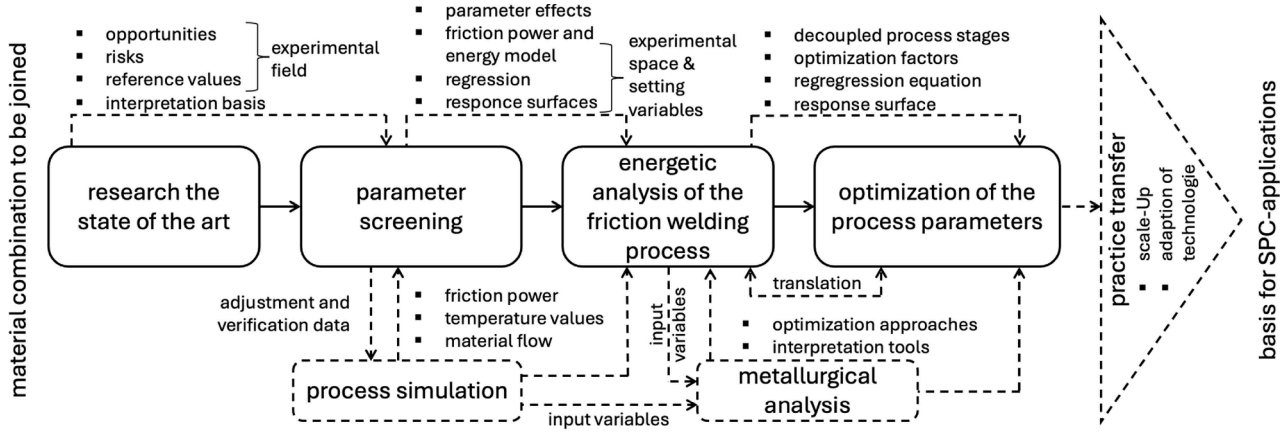

Fig. 1. Schematic representation of the analysis and optimization algorithm.

$$P_{fric} = \dot{En}_{fric} = \frac{dEn_{fric}}{dt} = M_{fric}\omega = M_{fric}2\pi n_{rot} \quad (2)$$

(Trommer, 2011; Seli et al., 2010)

$$En_{fric} = \int M_{fric}\, d\varphi = \int P_{fric}\, dt_{fric} \quad (3)$$

In addition to providing the required energy, the surfaces are cleaned during the frictioning stage, allowing the atomic grids to come into direct contact. According to Maalekian (2007), Oosterkamp et al. (2004), this fulfills all the conditions for bond formation. According to Pohle (1999) [therefore], adhesion with subsequent diffusion bonding occurs within a narrow joining zone when high forces are applied during the forging stage. This creates intermetallic compounds and metal bonds and thus ensures the material bond between the workpieces.

Although it is obvious and known that there is a clear functional separation between the frictioning and the forging stage, both cannot be analyzed separately by simply looking at the setting parameters. The reason for this are cross-stage, statistical interactions, which have a significant effect on the joining process for both similar and hybrid material joints (Winkler et al., 2023a). The resulting requirement to consider a large number of setting parameters inevitably leads to a high level of experimental effort when optimizing friction welding processes and makes interpretation of the results more difficult.

Because no approach for the complete decoupling of existing interactions between the frictioning and forging stage is currently documented for rotary friction welding with continuous drive, this paper presents such an approach. This is based on a statistical methodology and is to be verified with regard to its functionality using a hybrid aluminum-steel joint. The aim is to determine how the relationship between energy input and forge pressure affects the joint quality and whether it is possible to statistically decouple the frictioning and forging stage. By summarizing the parameters of the frictioning stage to friction power or energy, the statistical separation of the two process stages should enable an efficient analysis of the friction welding process with little experimental effort.

A statistical stage separation can be used to analyse frictioning stage parameters at constant forging. Subsequently, the forging stage can be optimised by substituting the frictioning stage parameters with the friction energy or the friction power in combination with the friction time. In the case of empirically conducted experimental series, this substitution prevents the double testing of different parameter combinations with identical friction power. When using statistical experimental designs, the potential for reducing the experimental effort results from the dependence of the number of required model constants on the number of analysed factors (N_F). In the case of full-factorial experimental designs, as they are often used for the calculation of regression models, the number of required experimental points (N_P) is exponential to N_F. Table 1 shows the formulae for calculating the number of design points for a full factorial Yates (4) and a central composite design (CCD) (5), which substantiate this statement. If these formulae are compared with the equations (6) and (7), which describe the increase in the number of design points (ΔN_P) when the number of factors is decreased by a value x, it can be seen that $\Delta N_P(x = z) > N_P(N_F{=}z)$. Consequently, splitting an experimental field into several smaller ones always saves experimental effort. Consequently, splitting a large experimental field into several smaller ones always saves experimental effort. A one-off determination of the friction power or friction energy and a subsequent substitution of the frictioning stage parameters with these representative substitute variables therefore offers the potential to save experimental effort. The prerequisite for this is that there are no interactions between the substituted parameters and the parameters analysed in the second instance.

Table 1
Formulas for calculating the number of experimental points for a full-factorial Yates or CCD experimental design (N_V) and their increase if the number of factors (N_F) is increased by the value x.

experimental design	Yates fully factorial		Central-Composite-Design	
number of design points (N_P)	$N_P(N_F) = 2^{N_F}$	(4)	$N_P(N_F) = 2^{N_F} + 2N_F + 1$	(5)
decrease of experimental effort per factor($\Delta N_P(x)$)	$\Delta N_P{=}2^{NF}(2^x{-}1)$	(6)	$\Delta N_P{=}2^{NF+x}{-}2^{NF}{+}2x$	(7)

The concrete reduction potential can be analysed on the basis of the numbers of design points shown in Table 2 for various factor quantities.

In addition to reducing the experimental effort, the harmonisation of the process analysis with the theoretical understanding facilitates the interpretation of generated results and the design of experimental design fields. An adequately comparable study for rotary friction welding with flywheel drive is documented in Wang et al. (2005). In Liu et al. (2020), Liu et al. prove significant differences between the process-related material influence in flywheel friction welding compared to the process variant with continuous drive, on the basis of which the results obtained can only be transferred to a limited extent. From Grant et al. (2009) it is known that dissipation influences workpiece heating and material plasticization. In the context of the scientific application, the effect of the intensity of the heat induction on the material flow, the thermal softening and the achieved joint quality is to be investigated by means of the presented approach. This energy-related process analysis could also represent the basis for a new type of process monitoring with a high degree of reliability.

Methods and materials

The general weldability of the research-relevant aluminum-steel joint has already been confirmed by documented research projects (Kawai et al., 2000). A comprehensive summary of the current state of research is documented in (Ghari et al., 2024; Ambroziak et al., 2014; Mehta, 2019; Murugan and Sathiya, 2023). It is known that this material combination only achieves industrially usable properties under optimized conditions and setting parameters (Wan and Huang, 2018; Li et al., 2006). The dependence of the welding result on the joining process design is attributed to the type and intensity of formation of intermetallic compounds (IMC) (Mehta, 2019; Kimura et al., 2017; Ambroziak, 1999). Since these are in any case considerably harder and more brittle than the base materials (Atabaki et al., 2014; Springer et al., 2011; Haidara et al., 2012), they inevitably cause a metallurgical weakening of the joining zone (JZ) (Ambroziak et al., 2014). In addition to the joint-forming IMC, the properties of the heat affected zone (HAZ) also have a direct influence on the joint strength. Depending on the process design, strength, ductility and hardness can vary, so that different joint properties are achieved (Mehta, 2019; Herbst et al., 2017; Taban et al., 2010; Reddy et al., 2008). According to Table 4, aluminum has significantly lower strength, a lower melting point and higher thermal conductivity than steel, so deformation and microstructural changes occur almost exclusively on the aluminum side (Wan and Huang, 2018; Seli et al., 2010; Herbst et al., 2017; Taban et al., 2010; Reddy et al., 2008). Although the latter are very complex, according to Abdulla et al. (2018), Wysocki et al. (2007) they can be reduced to the structural model shown in Fig. 3 on the left. Area (a) forms the thermally affected zone, areas (a)–(c) in their entirety form the mechanically affected zone. By the use of grid-based hardness mapping, the thermally and mechanically influenced zone [(a)] as well as the exclusively

Table 2
Number of experimental points as a function of the number of parameters investigated.

	Yates (fully factorial)					Central-Composite-Design				
N_F	2	3	4	5	6	2	3	4	5	6
N_P	4	8	16	32	64	9	15	25	43	77

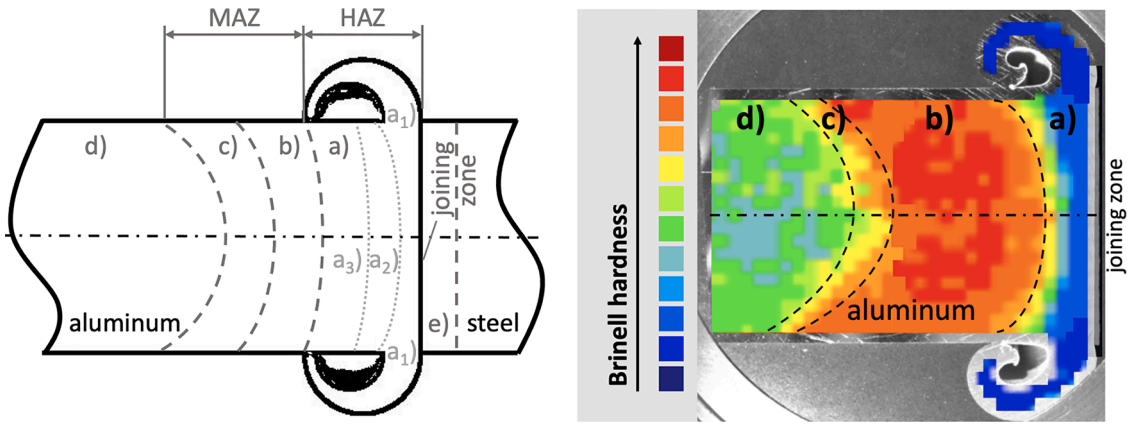

Fig. 3. The microstructural condition of the joining zone of friction-welded aluminum-steel joints [cf. (Wan and Huang, 2018), cf. (Wysocki et al., 2007), cf. (Ruge, 2013)]: (a) [thermally affected] fully plasticized zone; a_1) partially secondary recrystallized zone; a_2) recrystallized zone; a_3) partially recrystallized zone; b) plastically deformed zone; (c) partially plastically deformed zone; (d) undeformed zone; (e) [slightly,] (only) thermally affected zone.

mechanically affected specimen region [(b)-(c); MAZ], as shown in Fig. 3 on the right, can be visualized very well.

The correlations between the nature of the thermally and mechanically influenced area and the process parameters have not yet been scientifically investigated (Tasdemir, 2020). [For this reason], according to TASDEMIR, there is a great interest in investigating the energy input. [cf. (Tasdemir, 2020)] The present publication is intended to provide an approach for this.

Materials

For the aluminum component, the age-hardenable wrought alloy AA6060 according to DIN EN 573 (German Institute for Standardization (DIN), 2005) in heat treatment condition T6 is used. As the alloy has good strength, corrosion resistance and workability, it is suitable for a wide range of different applications, with the production of extruded profiles being the main use.

In the documented experiments, it is welded to the chromium-manganese alloyed case-hardening steel 16MnCr5, whose composition corresponds to the specifications of DIN EN ISO 683-3 (German Institute for Standardization (DIN), 2022). This steel material is frequently used in mechanical engineering for the manufacture of shafts and gear components. The specific material compositions and selected mechanical properties can be found in Tables 3 and 4.

Technological system

The experiments are carried out on a multivalent horizontal continuous drive friction welding machine. The forces occurring are recorded using the machine's internal sensors. This enables force-controlled execution of the process.

In the course of the experiment, rod-shaped semi-finished products with a diameter of 20 mm and a length of 100 mm are welded together. The aluminum workpiece is clamped on the slide side by means of a force fit in a turned-out two-jaw chuck. The clamping pressure is eight bar. The steel component is clamped on the rotor side, also force-fit at eight bar clamping pressure, in a turned three-jaw chuck. The aluminum workpiece is supplied axially to the rotating steel sample. The actual experimental setup is shown in Fig. 4.

Table 4
Test-relevant strength values.

material	R_m	hardness
AA6060	264 MPa	78 HB 2.5/6.25
16MnCr5	780-1080 MPa (Gomeringer et al., 2020)	176 HV10

In order to create a uniformly defined, clean joining surface in terms of both surface quality and spatial position, the steel sample is turned flat in the clamping position in preparation for welding. The average R_Z-value achieved is approx twelve micrometers. The friction surfaces of the aluminum specimen are adequately machined in preparation for the experiment and are cleaned with ethanol immediately before welding.

Welding process and its parameters

As a distance-controlled process can be designed to be much safer than a time-controlled one in terms of workpiece shortening, it is generally more suitable for carrying out screening programs. This applies even more to friction welding of aluminum alloys due to their low strength. The process is therefore designed to be force-controlled and distance-controlled so that friction time is transformed into a secondary variable. Since it is known from theory that, in principle, a distinction is only made between an excessively short and a sufficiently long forge time, these setting variable is eliminated as influencing variable by a generally high setting. This results in the system model shown in Fig. 5 for the screening experiments.

The setting values documented in Table 5 are used for the constant process and control parameters, which always remain unchanged during the tests:

The set-up times describe the set ramp times for reaching the respective target force value. Due to the low strength of the aluminum material, an inertial frictioning stage is not used.

Design of experiments

The investigations are based on a regressive process analysis. In addition to the basic determination of achievable value regions for the target variables, the first step is to generate a response surface for the

Table 3
Compositions of materials (German Institute for Standardization (DIN), 2005, 2022).

material	Si	Fe	Mg	Zn	Cu	Cr	Mn	C	Ti+Zr	Al	div.
AA6060	0.3-0.6	0.1-0.3	0.1	0.15	0.1	0.05	0.1	0	0.1	bal.	0.15-0.3
16MnCr5	0.4	balance	0	0	0	0.8-1.1	1-1.3	0.14-0.19	0	0	0.06

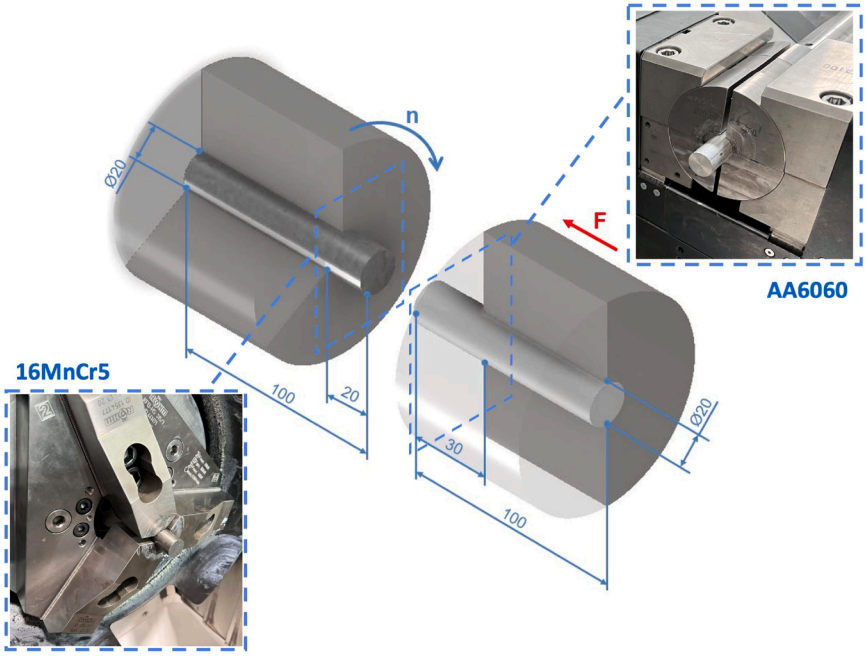

Fig. 4. Technological experiment setup.

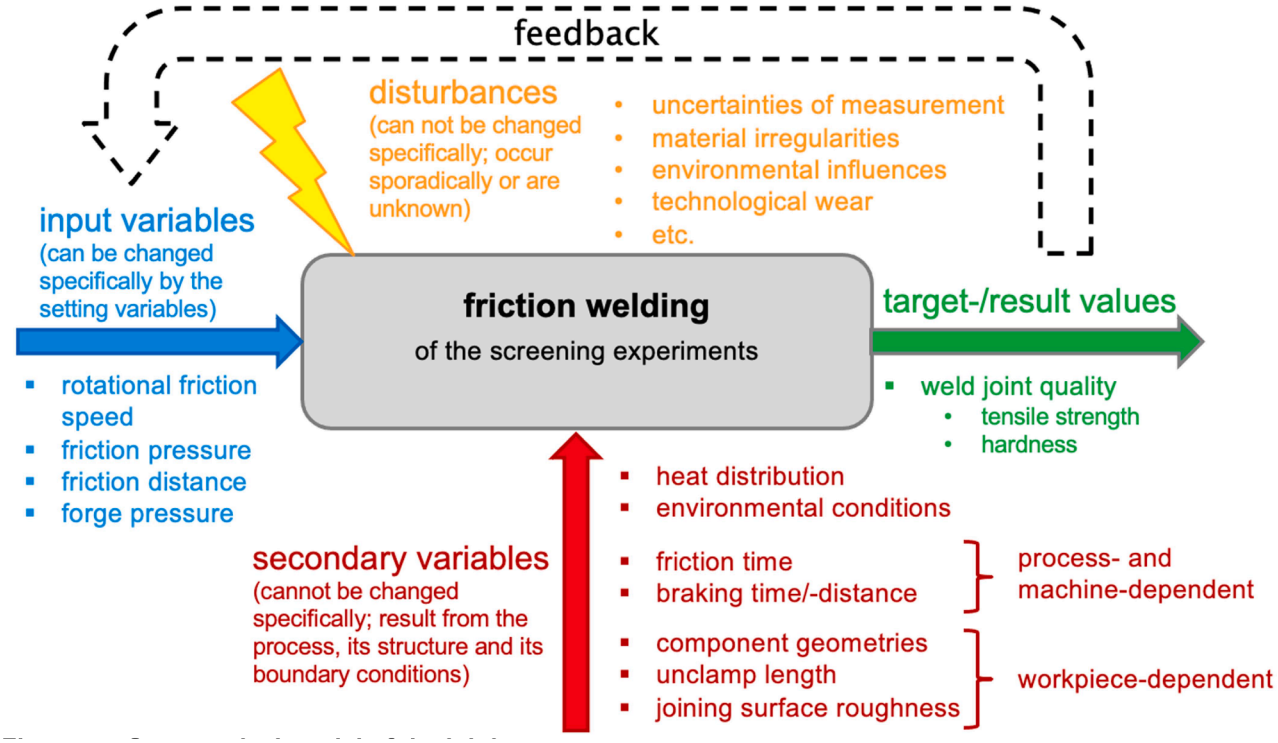

Fig. 5. Systematical model of the joining process.

Table 5
Constant process parameters of the friction welding experiments.

process parameter	set-up times		forge time	rotational forge speed
	frictioning [$t_{fric\ set\text{-}up}$]	forging [$t_{forge\ set\ up}$]	[t_{forge}]	[n_{forge}]
setting value	0.01 s	0.1 s	5.0 s	0 min^{-1}

induced friction power.

The design of the experimental field corresponds to the variant of the central composite design shown in Fig. 6.

As already mentioned in Winkler et al. (2023b), the combination of inscribed and face-centered experimental points of the axial design component makes it possible to detect potentially existing nonlinearities with a high degree of certainty. In addition, unlike with an extended axial component, the entire experimental field can be analyzed full factorial. Measured in terms of the informative value of the model, the

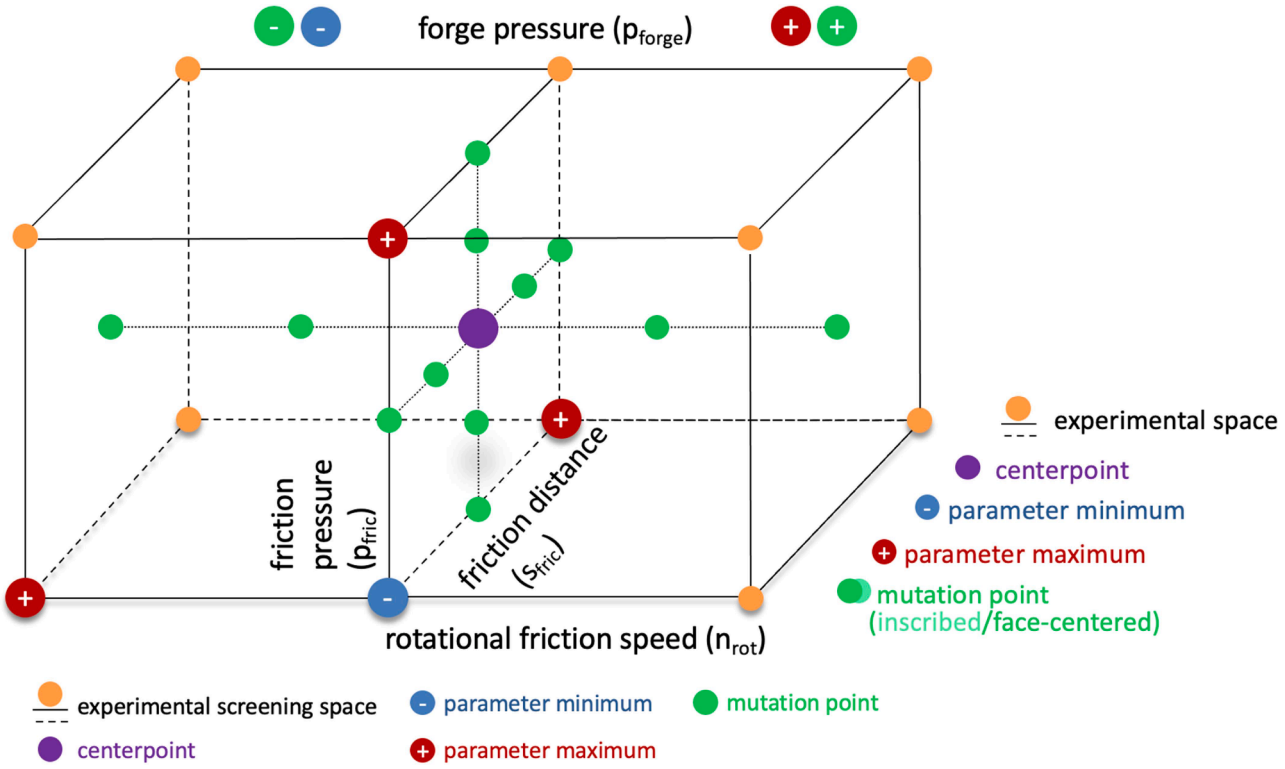

Fig. 6. Design of the process analysis.

field size of 25 experimental field points can be considered acceptable. For the purpose of statistical validation, the factorial field points and the center point are verified five times, the axial points three times. The five-level testing of each setting parameter provides a meaningful basis for a quadratic regression model according to (8). If required, a linear or cubic model can be derived from this.

$$y = \bar{y} + \overbrace{\sum_{i=1}^{N_F} \frac{E_i}{2} x_i}^{y_{main}} + \overbrace{\sum_{i=1}^{N_F-1} \left(\sum_{j=i+1}^{N_F} \frac{E_{ij}}{2} (x_i x_j) \right)}^{y_{interact}} + \overbrace{\sum_{i=1}^{N_F} \frac{E_{ii}}{2} (x_{ii})^2}^{y_{dim}} + \overbrace{\sum_{P=1}^{N_P} \frac{1}{N_\varepsilon} \sum_{i=1}^{N_\varepsilon} (y_{Pi} - \overline{y_P})^2}^{\varepsilon} \quad (8)$$

(Winkler, 2023)

y	*(functional) value of the target variable/quality characteristic*
$\bar{y}$	*average value of the target variable/quality characteristic*
y_{main}	*direct influence of the setting parameters*
$y_{interact}$	*mutual influence of the setting parameters (interactions)*
y_{dim}	*components dependent on the dimension of the model (non-linearities)*
ε	*influence of the disturbance variables*
E_i	*main effect of the input values*
E_{ij}	*interactions of the input variables*
N_F	*number of factors*
N_P	*number of experimental design points*
N_ε	*number of verifications per point*
x_i, x_j	*normalized setting value of the setting parameter; range: [−1;1]*
$\overline{y_P}$	*average value per experimental design point*
y_{Pj}	*single measured value*

The design of the experimental field bases on the standard specifications for similar welds of the aluminum alloy in German Welding Society (DVS) (2011). The forging stage is dimensioned in such a way that the maximum specimen load occurs in the area of the yield point. In order to be able to detect potential influences of the forge pressure on the braking stage, the former is also varied, although it does not represent a setting parameter of the frictioning stage. Table 6 documents the specific parameter values.

The statistical evaluation contains a significance test of all setting parameters with a confidence interval of 95 percent. Finally, the influences of all control variables on the joint strength and the induced friction power are quantified by calculating the main and interaction effects.

The regressively determined response surface of the applied friction power is used to derive a design of experiments and a resulting regression model for analyzing the interaction of the friction power, the friction time and the forge pressure. The resulting experimental design causes a change in the systematic input parameter model and enables a separate consideration of the frictioning and forging stage according to Fig. 7.

Because the two setting parameters, friction power and friction time, according to (3) define the kinetic energy, which is converted into thermal energy by the process-related friction, the statistical investigation of energetic influences is no longer carried out using distance-based but friction-time-based process control. Fig. 8 shows the designs used in the second iteration. These result in the experimental plan shown in Table 8.

Metallurgical analysis and determination of the mechanical joint quality

In order to detect any thermal effects on the material strength and assess their impact, a HBW 2.5/6.25/10 microhardness mapping is carried out. The offset to the joining zone and the edge zones is 0.5 mm. The measuring points are arranged in a grid of 0.8 × 0.8 mm.

During the tensile tests in accordance with ISO 6892-1 (German Institute for Standardization (DIN), 2020), the specimens are continuously stretched to absolute failure at a rate of ten millimetres per minute. The maximum tensile force is used as the evaluation criterion. To produce uniform profiles, the weld flash is turned as shown in Fig. 9 and the joining area is reduced to a diameter of 18 mm. The weld specimens are clamped on both sides in precisely fitting round profile recesses. In order

Table 6
Limit values of the experimental field (coloring according to Fig. 6).

parameter		unit	minimum	negative mutation	average	positive mutation	maximum
rot. friction speed	**(n_{rot})**	[min^{-1}]	500	875	1.250	1.625	2.000
friction pressure	**(p_{fric})**	[MPa]	20	40	60	80	100
friction distance	**(s_{fric})**	[mm]	3.5	4.375	5.25	6.125	7
forge pressure	**(p_{forge})**	[MPa]	50	80	110	140	170

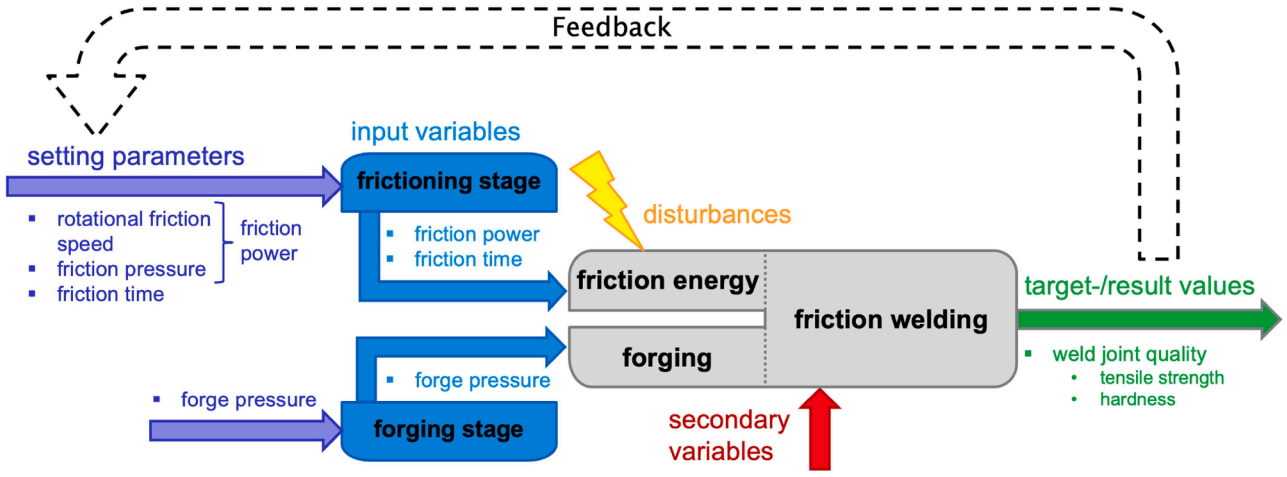

Fig. 7. Systematic model of energetic analysis.

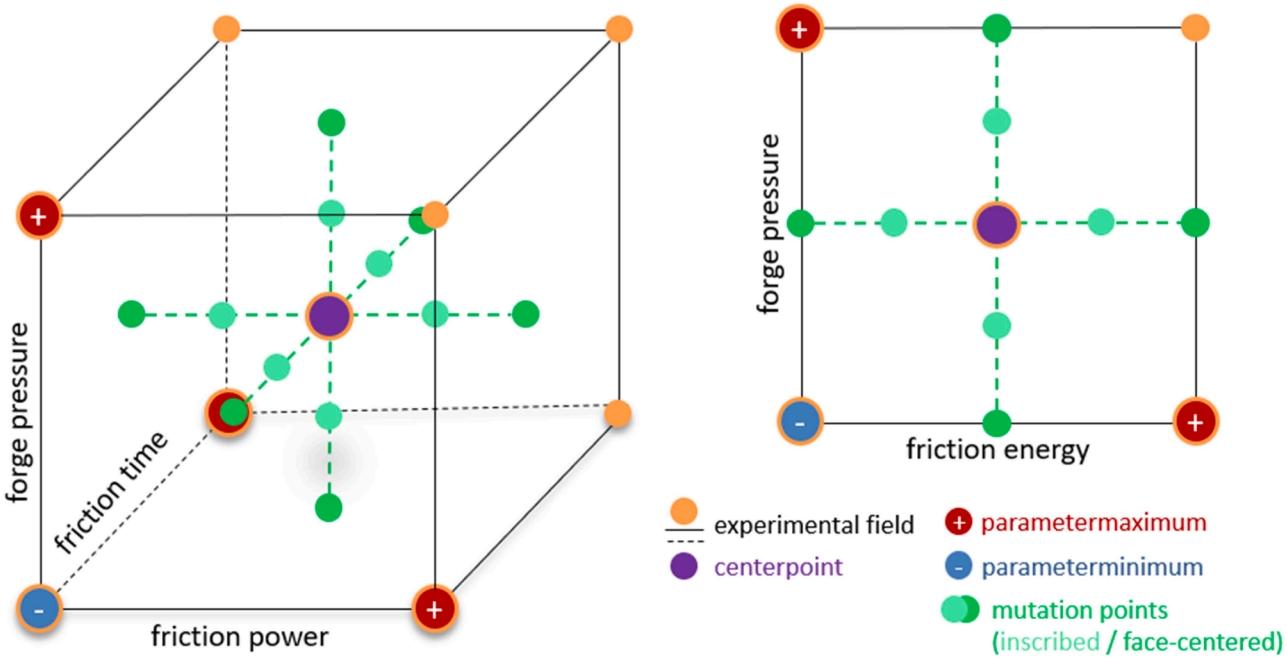

Fig. 8. Experimental design of the energetic investigation.

to rule out any influence of ageing processes on the test results, the specimens are always post-processed and the tensile tests are always carried out within a time window of 48 h after welding.

To support the interpretation of the results, both the weld sample cross-sections and the fracture surfaces are examined visually under a scanning electron microscope (SEM).

Three-point bending tests according to ISO 7438 (German Institute for Standardization (DIN), 2000) with an infeed speed of five

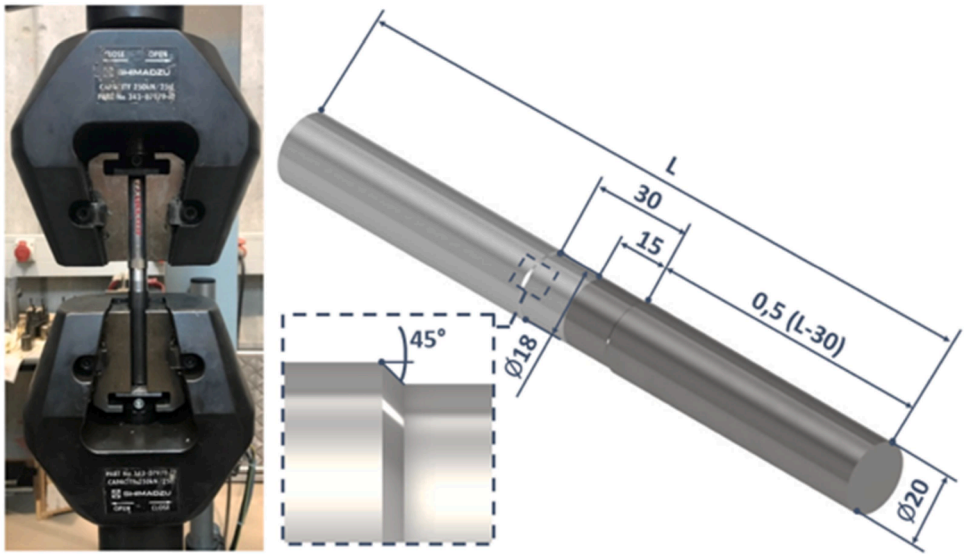

Fig. 9. Experimental setup and specimen geometry of the tensile tests.

millimeters per minute are carried out for selected specimens. During preparation, the weld flash is turned down to a diameter of 20 mm, resulting in cylindrical specimens.

Simulation of the friction welding process

Although Eqs. (1) and (3) provide a general insight into the friction welding process, they can only be solved analytically with considerable simplifications. The numerical process simulation "virtua RFW" uses the finite element method to predict quantitative results for arbitrarily complex process variables, such as workpiece shortening, frictional torque or heat induction, which are investigated and discussed in chapter"Energetic Investigation of the Friction Welding Process". As torques and temperatures cannot be recorded by the used sensors, the application of simulative software enables a more in-depth process analysis. The physical simulation model is based on the principle of virtual velocities and temperatures and is able to calculate both the transient temperature field (θ) and the displacement field (u). The challenges are in the material description, the friction modeling, the treatment of large deformations and the processing of constantly changing states. For a detailed description of the mathematical and physical principles, please refer to Schmicker (2015). The agreement of simulated in-process variables with real values was verified selectively in the course of preliminary experiments.

Sensitive process analysis

Results

All tested parameter combinations produced a stable, material bond between the two joining partners. Based on the variance analysis, Table 7 lists the significant parameters for the qualitatively and energetically relevant results as well as the associated effects according to their significance. The temperature values used for the calculation were determined by simulation.

Based on the comparatively high significance of the interaction effect of both stage pressures, the difficulty in separating the frictioning and forging stage is made clear when considering the setting parameters alone. When analyzing friction welding processes, it is important to always consider the braking time. Although it is a secondary variable, it can influence the effective duration and amount of heat induction and therefore the welding result. Within the analyzed experimental field, it averages 0.4 s with a variance of 0.2 s. The influence of the braking time is therefore considered negligible. Its influence is therefore assessed as negligible, but can certainly play a role when transferring the process to a more massive machine [cf. (Ochi et al., 1993)]. The measured friction time comprises the time span from component contact until the specified friction distance value is reached. Consequently, it is dependent on all parameters of the frictioning stage.

The response surfaces of the measured joint tensile strengths illustrated in Fig. 10 show that a high forge pressure can mitigate the effects of a suboptimal frictioning stage design and stabilize the process accordingly. The finding that the joint strength is positively influenced by a high forge pressure level is confirmed in Winkler et al. (2023a), Abdulla et al. (2018), Senthil Murugan et al. (2020), Irawan et al. (2017), Kimura et al. (2005).

By using the simulation software, the average prevailing friction power can be determined from the friction torque curves according to Formula (2). As expected, this depends on the rotational friction speed and the friction pressure. Fig. 11 shows the interaction between rotational friction speed and friction pressure in the form of a response surface. In order to compare these with the theoretically calculated expected torque values, M_{fric} is calculated from (2) using the relevant setting variables as follows:

Table 7
Results of the ANOVA (significant setting parameters and their effects).

target value		significant parameters (size of the effect)					
		1	2	3	4	5	6
ultimate tensile strength	**(σ_{tens})**	p_{fric} (35.48)	p_{forge} (22.0)	p_{fric} x p_{forge} (−18.69)	n_{rot} (12.68)		
friction time	**(t_{fric})**	p_{fric} (−4.31)	n_{rot} (−1.82)	n_{rot} x p_{fric} (1.67)	s_{fric} (1.29)		
braking time	**(t_{brake})**	n_{rot} (0.24)	p_{fric} (−0.06)	n_{rot} x p_{fric} (−0.02)			
friction power	**(P_{fric})**	p_{fric} (8.24)	n_{rot} (6.74)	n_{rot} x p_{fric} (5.28)	s_{fric} (−1.17)	n_{rot} x s_{fric} (−1.17)	p_{fric} x s_{fric} (−0.98)
friction energie	**(En_{fric})**	p_{fric} (−1.16)	s_{fric} (2.61)				
max. joining zone temperature	**($T_{HAZ\ max}$)**	n_{rot} (55.57)	s_{fric} (15.02)	p_{fric} (−12.73)	n_{rot} x s_{fric} (−13.13)		

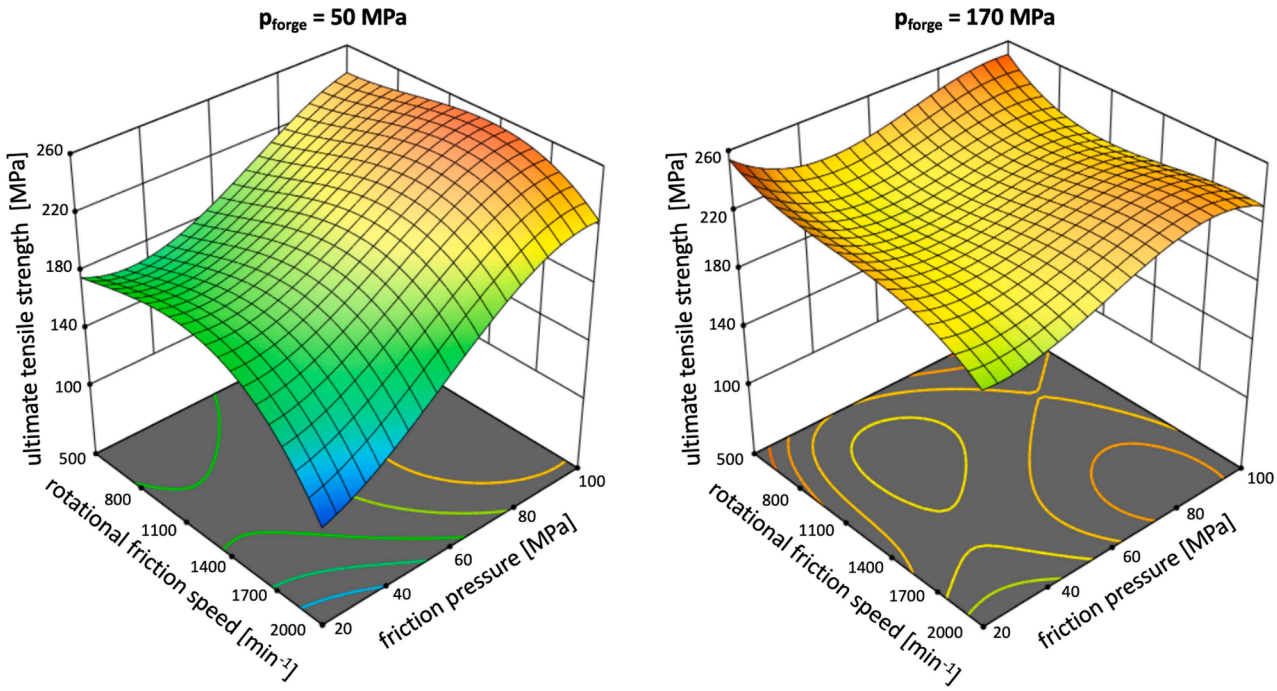

Fig. 10. Influence of the rotational friction speed and the friction pressure on the tensile strength of the friction welded joint at different forge pressure levels.

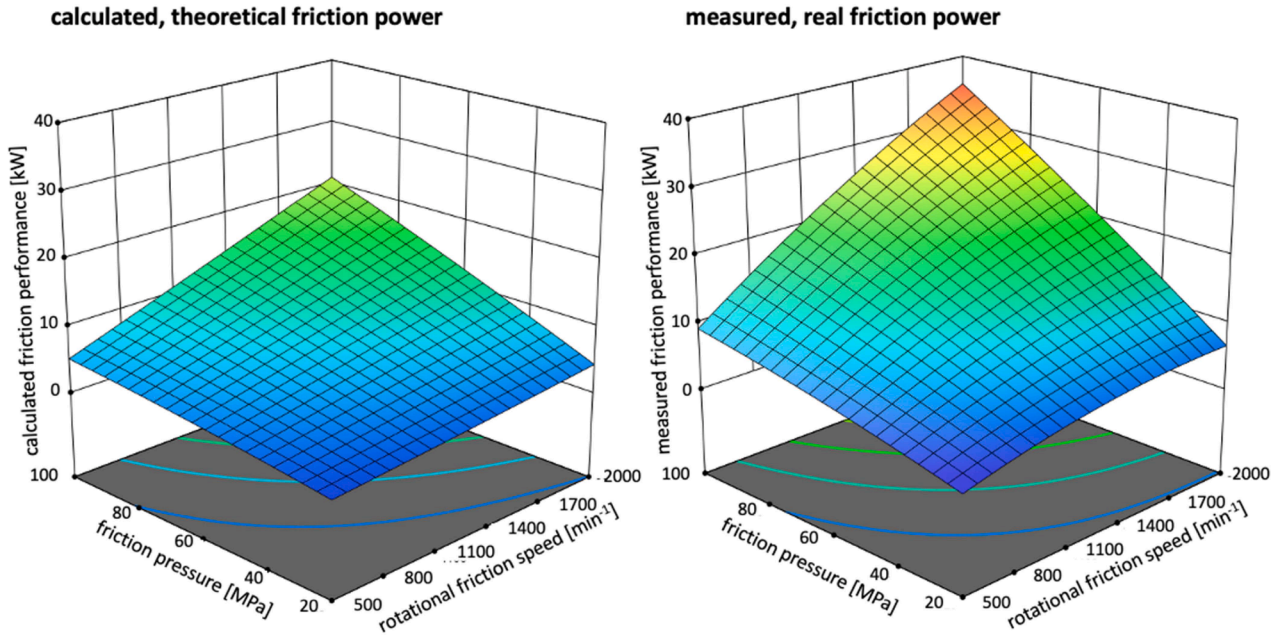

Fig. 11. Discrepancy between the response surface calculated using (2) resp. (10) (left) and the experimentally determined response surface (right) to illustrate the influence of rotational friction speed and friction pressure on the friction power.

$$dM_{fric} = dF_{fric} r \tag{9}$$

(Trommer, 2011), vgl.20

$$M_{fric} = \frac{2}{3}\pi\mu r^3 p_{Reib} \text{ (for round solid cross – sections)} \tag{10}$$

(Trommer, 2011), vgl.20

There is a clear discrepancy between the friction power data predicted mathematically using (2) with (10) and the friction power data determined experimentally and simulatively. This discrepancy is attributed to the inconsistency of the force curves, especially during the contacting and braking stages, as well as the inconsistency of the material and joining surface properties during the process. While the mathematical Eqs. (2) and (10) represents a stationary state,[d] these effects are taken into account in the experimentally supported regression model. Since the intensity of the effects mentioned increases with increasing friction pressure, a prior, test-based determination of the friction power behavior is recommended, especially when researching friction welding processes at an intensive friction power level.

[d] constant coefficient of friction μ=0.1; n_{fric} and p_{fric} correspond constantly to the respective setting value acc. to Table 6

As already shown in formula (3), the frictional energy is influenced by the friction time. Fig. 12 illustrates the ultimate tensile strength values detected in the sensitive process analysis in relation to friction time levels above and below two seconds.

It should be noted that the previously explained influence of the braking time does not play a role in the power or energy-related analysis, as the time required for spindle downtime is already included in the results as long as the production system is not changed.

In accordance with the simulatively generated response surface shown in Fig. 13, the upper limit of the induced energy is set at 40 kJ in the course of further experiments. Because the friction pressure according to Table 7 has the strongest influence on the friction time of time-controlled processes or the shortening of distance-controlled processes, such amounts of energy can only be realized with low friction pressures. Fig. 13 illustrates this. The response surface of the induced energy amount shown therein is constant at a low level at high friction pressure.

Because of the excessive shortening, long friction times at a high friction pressure level cannot be investigated. Since the variance of strength values achieved according to Fig. 12 also varies greatly in the case of a long frictioning stage, the duration of the energetic analysis is limited to a maximum of two seconds.

However, an excessively high ratio of rotational friction speed to friction pressure can cause heat build-up. The combination of intense friction and low shortening speed heats up the joining zone to the extent that it can become brittle and the joint strength deteriorates (Yamamoto et al., 2004; Ikeuchi et al., 2005; Yamamoto et al., 2007). This effect is intensified with increasing friction time. According to the simulated response surface in Fig. 14, a high joint strength with good process stability can be achieved in a joining temperature range between 500 °C and 600 °C. Overheating of the joining zone should be avoided in order to achieve high joint strength [cf. (Seli et al., 2010)]. In accordance with this, it is shown in Bouche et al. (1998), Jank et al. (2008) that the resulting IMCs are drawn into the base material like stems at a joining temperature of 500 °C and above. Due to the complete insolubility of aluminum and iron, these IMCs deviate structurally from the base materials according to Gottstein (2007) and only have a limited homogeneity range compared to them. As a result, the joining zone is increasingly weakened with increasing joining temperature, even far from the IMC.

The rotational friction speed and friction time level are therefore limited for further experiments so that overheating of the joining zone is avoided. According to the Pearson coefficient in Formula (11), the maximum joining zone temperature correlates to 79.7 percent with the rotational friction speed, so it is advisable to declare the rotational friction speed as the determining factor with regard to the energy input or the frictioning stage and to adapt the friction pressure to this depending on the desired friction power level.

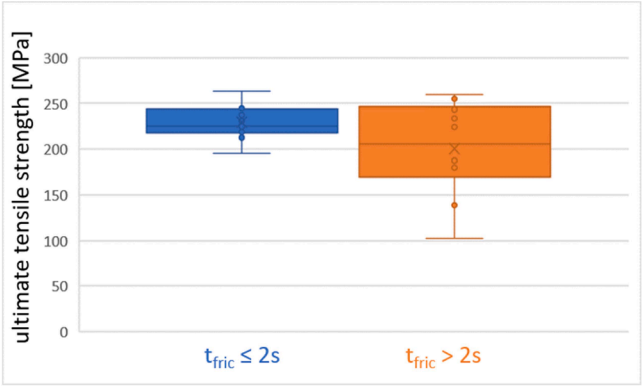

Fig. 12. Influence of friction time on the tensile strength of the screening specimen.

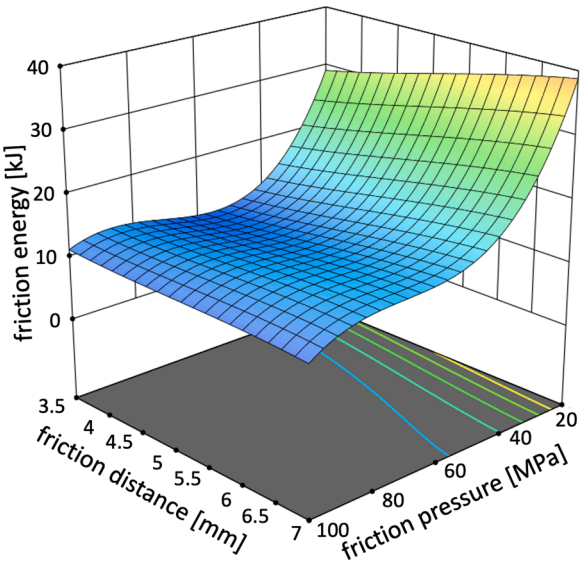

Fig. 13. Influence of friction pressure and friction distance on the friction energy.

$$Cor = \frac{\sum (x_i - \bar{x})(y_i - \bar{y})}{\sqrt{\sum (x_i - \bar{x})^2 \sum (y_i - \bar{y})^2}} \tag{11}$$

A similar relationship between rotational friction speed and joining zone temperature is described in Wang et al. (2005) for friction flywheel welding. The high correlation between rotational friction speed and joining temperature can be attributed to the self-regulation of the friction welding process. According to (1), the frictional moment and the frictional pressure are limited because, according to Lotz (2013), an equilibrium of mechanical hardening and thermal softening always occurs during the frictioning stage. According to (2), this self-regulation does not apply to the rotational friction speed, for which reason it has a stronger effect on the joining temperature. The proven influence of the rotational friction speed on the welding temperature confirms the transferability of the findings from Sasmito et al. (2023), Ikeuchi et al. (2005) regarding monolithic aluminum weldings to adequate mixed joints.

Discussion

The screening experiments once again confirm the process-side link between the frictioning and forging stage with regard to joint strength and the cross-stage interactions that cause this. However, concrete correlations could only be derived to a limited extent due to the latter. Nevertheless, it is clear that the frictioning stage parameters influence the joining temperature as well as the material flow and thus also the joint quality achieved. The focus of the research was on the generation of the friction power response surface, which forms the basis for the subsequent energetic investigation of the friction welding process. As significant differences were found between the experimentally determined and the mathematically calculated friction power behavior, it was essential to carry out these preliminary tests.

Energetic investigation of the friction welding process

Results

Suitable combinations of rotational friction speed and friction pressure are selected from the experimental determined friction power regression shown in Fig. 11 (right) in order to achieve the required friction power for the experimental field defined in Table 8. The

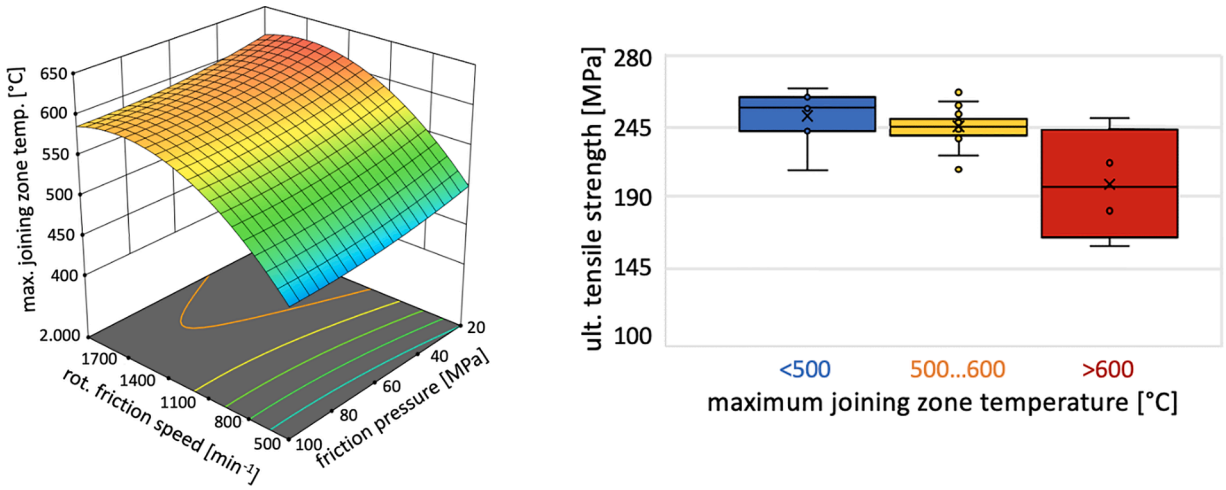

Fig. 14. Influence of the rotational friction speed and friction pressure on the joining zone temperature (left) and the influence of the joining zone temperature on the joint strength (right).

Table 8
Limit values of the experimental field of the energetic investigation.

parameter		unit	minimum	negative mutation	average	positive mutation	maximum
rot. friction speed	**(n_{rot})**	[min^{-1}]	831	719	987	838	1.132
friction pressure	**(p_{fric})**	[MPa]	27.9	54.8	19	99 2	99.8
friction power	**(P_{fric})**	[kW]	5	7.1	10	14.1	20
friction time	**(t_{fric})**	[s]	0.5	0.875	1.25	1.625	2
forge pressure	**(p_{forge})**	[MPa]	50	82.5	115	147.5	180

individual field points are verified in the same way as the first series of experiments (Table 9).

To ensure a uniform energy input, the difference between the contact torque and the average friction torque should be as small as possible when creating the experimental field. The rotational friction speed should therefore be set as high as possible, taking into account the thermal conditions. As the strength values of the previously performed screening, as shown in Fig. 15, have a strong divergence and their maximum only at low friction forces, friction energy and friction force are considered logarithmically according to Figs. 16–18.

The evaluation of the statistical effects of the energetic experimental field shown in Table 10 shows no significant interaction effects between parameters of the frictioning stage and the forge pressure. The desired statistical separation of the two process stages has therefore been achieved.

Although the achieved tensile strength according to (11) correlates to 85.8 percent with the induced friction energy, the high interaction effect between friction power and friction time indicates that the type of energy input is also highly relevant and should be considered. The energy-related evaluation of the experimental field shown in Fig. 16 in accordance with Table 8 shows that a high energy input tends to lead to a higher joint strength. However, the high heat input and the long frictioning stage required for this also result in greater shortening of the aluminum workpiece.

As already shown by the effects in Table 10, the joining zone temperature is strongly dependent on the generated friction power. An examination of the thermal states in Fig. 17 shows the effect for the two experimental field limits.

It is important to note the power range $\Delta P_{fric1} = 0 \ldots 7$ kW and the power $P_{fric2} = 14$ kW at high friction time, as these result in very uniform heating of the joining zone, whereby the centre area always experiences less heating due to rotational speed dependence. A comparable phenomenon is confirmed in Wang et al. (2005). In the case of a high friction power (P_{fric2}), this leads to a higher temperature and thus to increased soft annealing effects, which reduce the joint strength despite the high energy input. At low friction power (ΔP_{fric1}) and lower joining temperature, a stable experimental field zone is created, as shown in Fig. 18, in which high joint strengths are generated. The local characteristics of this area are at their maximum at a forge pressure of $p_{forge} = 160.5$ MPa. The results of the hardness mapping carried out in accordance with Chapter *"Metallurgical Analysis and Determination of the mechanical Joint Quality"* illustrate the effects on the material flow and the nature of the HAZ. It can be recognized that, according to Wang et al. (2005), the process-dependent thermal fields cause lateral softening of the material in the joining zone.

Table 9
Results of the energy ANOVA (significant setting parameters and their effects).

target value		significant parameters (magnitude of the effect)			
		1	2	3	4
ult. tensile strength	**(σ_{tens})**	P_{fric} (−35.86)	P_{fric} x t_{fric} (44.82)	t_{fric} (−8.47)	p_{fric} (42.27)
max. joint zone temperature	**($T_{HAZ\ max}$)**	P_{fric} (84.28)	t_{fric} (33.49)		

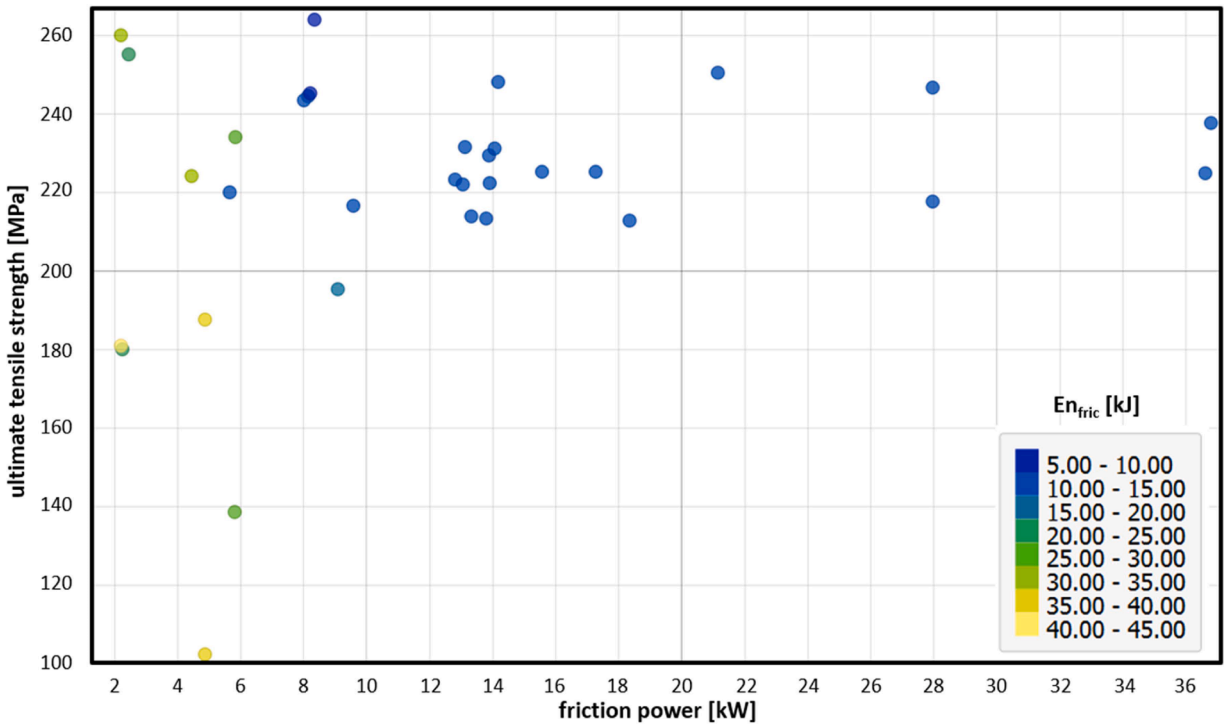

Fig. 15. Influence of friction energy and power on the tensile strength of screening specimen.

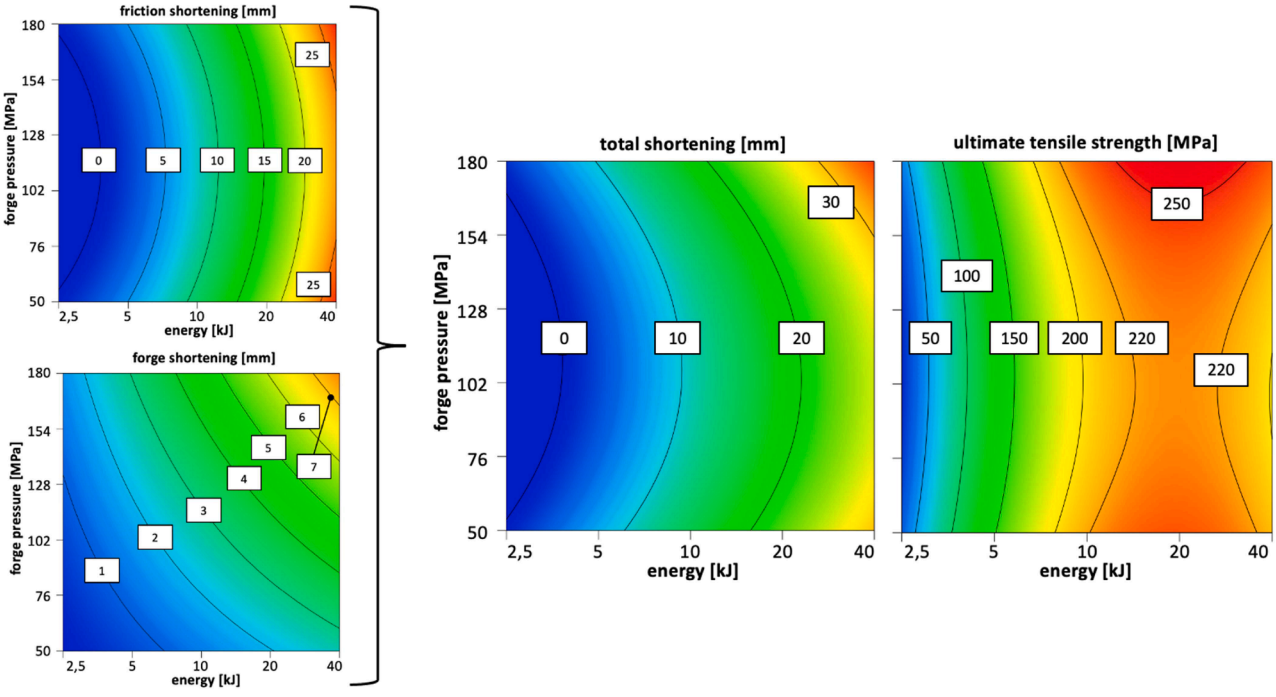

Fig. 16. Influence of friction energy on friction-, forge- (left) and total shortening (center) as well as tensile strength (right).

According to the findings of Hincapié et al. (2020), the less intensive joining zone heating with moderate energy induction results in a deviating flow behavior of the aluminum material. A lower friction power leads to a thicker weld flash, which does not bulge like a basket handle but is pushed over the edges of the steel joining partner. A comparable influence of rotational friction speed and torque on the weld flash is described in Wang et al. (2005). The illustration of the simulated material flow in Fig. 19 makes it clear that this results in a shift of the position of the highest equivalent plastic strain, which according to Tasdemir (2020) also influences the material recrystallization, from the specimen center (Alves et al., 2010) to the lateral area. The intensity of the deformation is also significantly reduced.

As a result of the altered flow behavior at low friction power, compressive tensions and congruent with (Bendzsak et al., 1997) shear effects occur around the outer edges of the steel profile, which partially harden the aluminum and prevent the formation of lateral softening

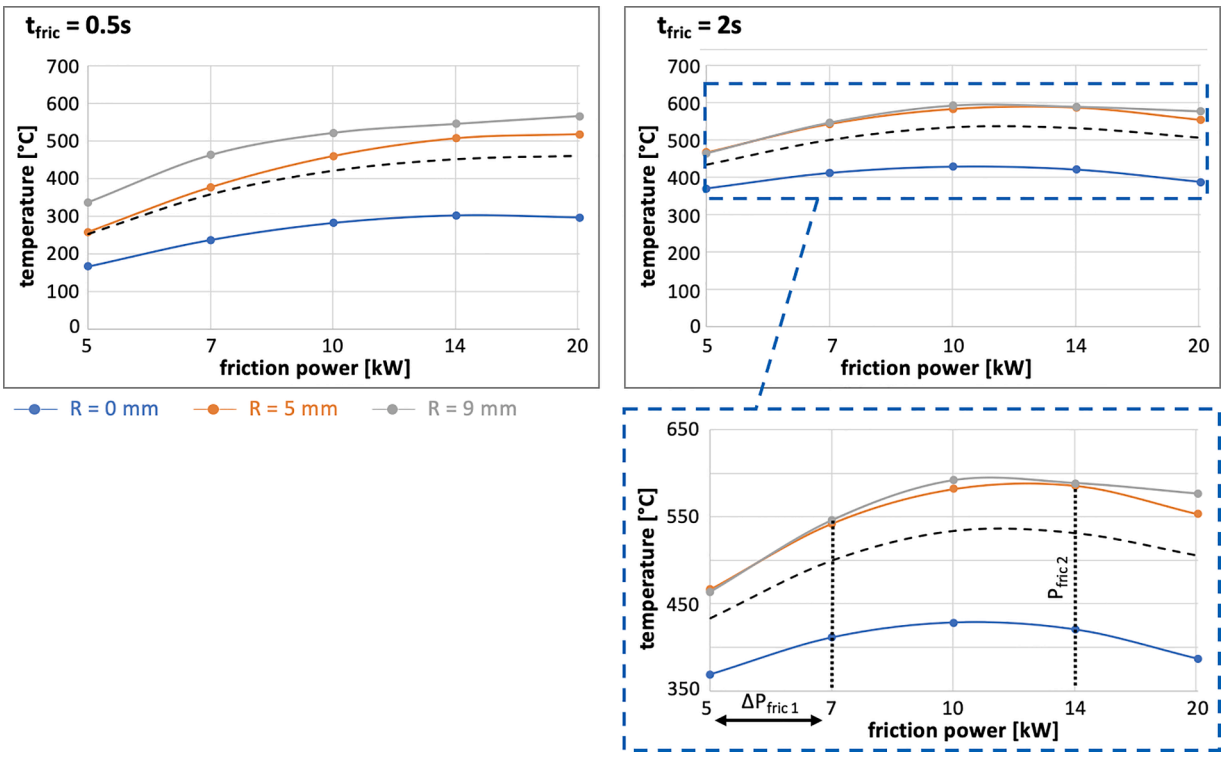

Fig. 17. Simulatively determined joining temperatures in different radial areas of the joining surface (center: $R = 0$ mm; outside: $R = 9$ mm) with various friction power and friction time.

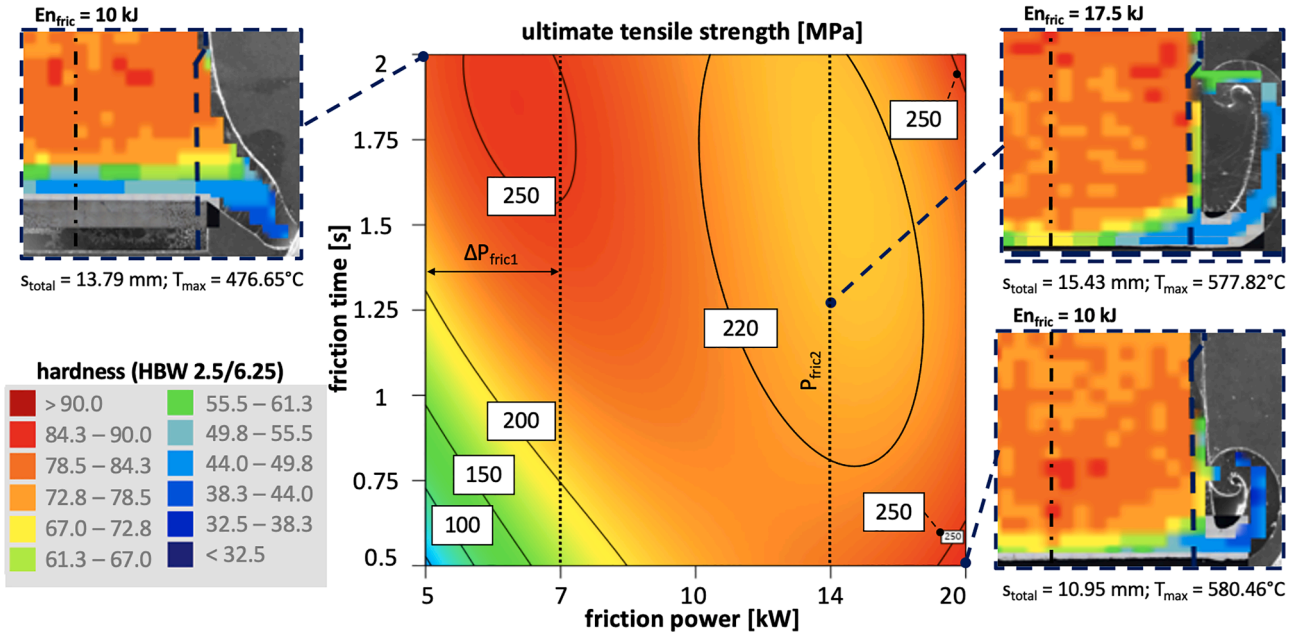

Fig. 18. Friction time - friction power response surface at $p_{forge} = 160{,}5$ kW and selected hardness curves.

Table 10
Crack and necking depths of the HAZ and JZ according to Fig. 22.

friction power [P_{fric}]	friction time [t_{fric}]	HAZ constriction [ΔD_{HAZ}]	crack depth JZ [ΔD_{JZ}]
20 kW	0.5 s	3.17 mm	1.33 mm
8 kW	1.5 s	2.36 mm	0 mm

notches. The zone of least hardness therefore shifts to the radial center of the aluminum sample. Such phenomena have already been observed by authors during friction welding of pipe cross-sections in Kawai et al. (2000).

Excessive heating over a longer period of time results in an overly intensive formation of the heat affected zone and the radial softening notches it contains. As Fig. 20 illustrates, these cause a weakening of the joint tensile strength and confirm the relationship between flow behavior and joint strength already proven in Wan and Huang (2018).

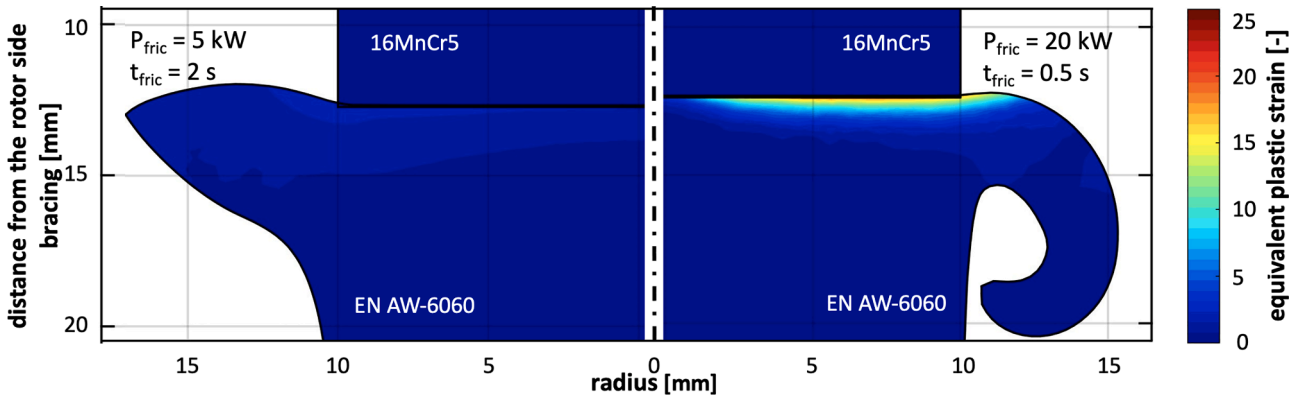

Fig. 19. Material deformation with different friction power/friction time ratios.

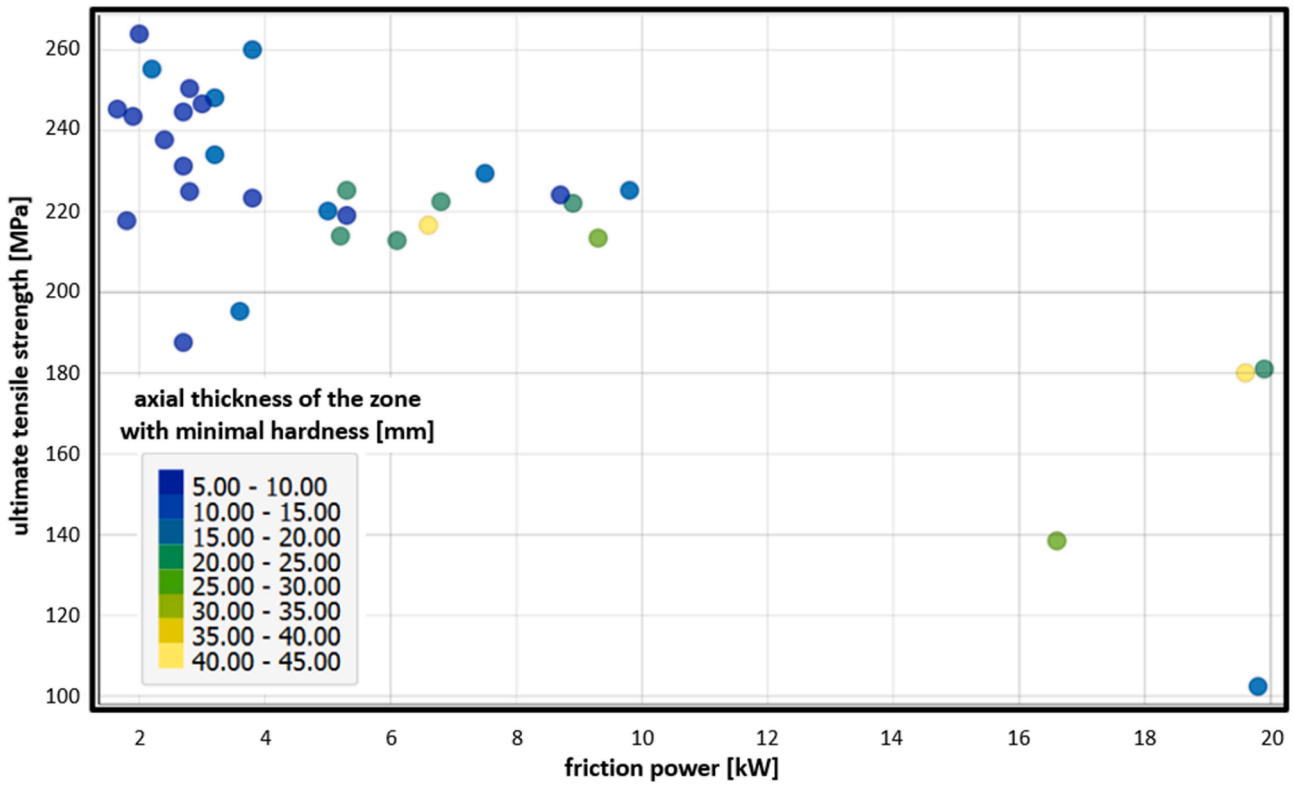

Fig. 20. Influence of the HAZ characteristic on the ultimate tensile strength of the joint.

A numerical-experimental optimization iteration takes a closer look at the moderately heated zone of high strength (P_{fric} = 5…8 kW; t_{fric} = 1.5…2 s) from Fig. 18. On average, tensile strengths of 240 MPa are measured within the experimental field, which have a standard deviation of 17,65 MPa. The optimum determined by mathematical enumeration represents a friction power of P_{fric} = 8 kW with a friction time of t_{fric} = 1.5 s. As Fig. 21 illustrates, this combination of parameters produces a very homogeneous HAZ, which acts as a ductile compound layer. Compared to the industrially standard power-intensive short-time welded specimen, higher joint strengths can be achieved.

It is clear that by applying a moderate friction power, it is possible to induce a higher amount of energy with less overall shortening. In combination with the mechanical mechanisms explained above, this significantly stabilizes the joint zone. In addition, the thermally influenced zone has a significantly higher ductility. Fig. 22 compares the failure behavior resulting from both with that of the established industrial standard (high friction power, short friction time (Reiners and Kreye, 1988; Shinoda et al., 2001)).

The progression of the stress-strain curves in Fig. 23 and the measured values in Table 10 illustrate the mechanical effects of the lower cross-section reduction. As a result of the lack of crack formation in the radially outer specimen zone, the elastic deformation is maintained at much higher load ranges than is the case with short-term, power-intensive welding.

Due to thermal softening, the failure of the weld specimens always occurs in the heat-affected zone along the joint surface. Occasionally, fragments are broken out of the aluminum workpiece and remain on the steel surface. The results of the bending test shown in Fig. 24, clearly show that the joining zone area is much more ductile when using the optimized parameter combination, which leads to higher process stability. The combination of homogeneity and low hardness leads to a lower support effect of the central specimen area in the bending load case. In contrast to the tensile test, no improvement in strength is therefore achieved.

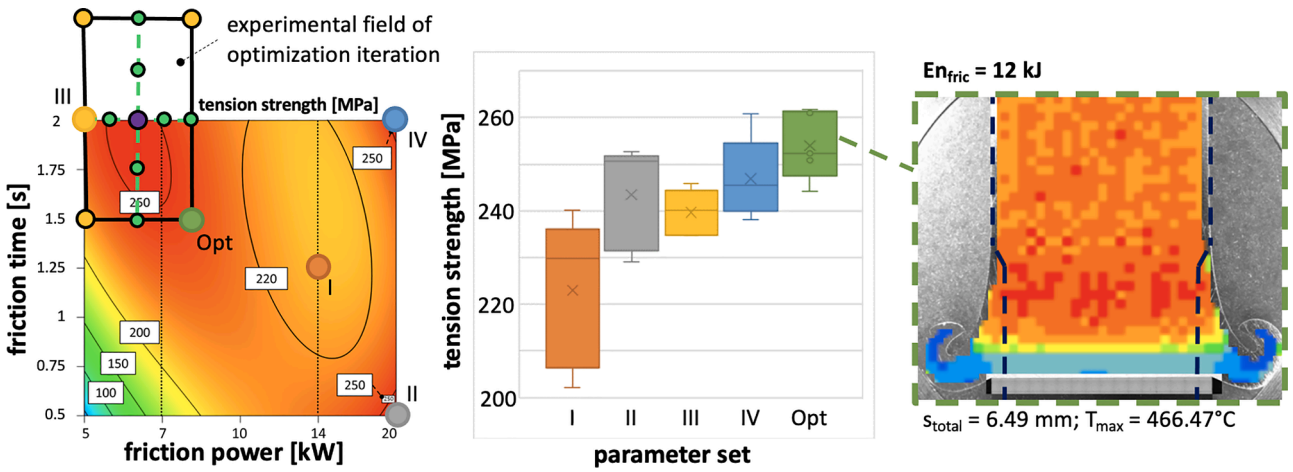

Fig. 21. Comparison of achieved ultimate tensile strengths with intensive-short-term and moderate-long-term energy induction (hardness progression scale analogous to Fig. 18).

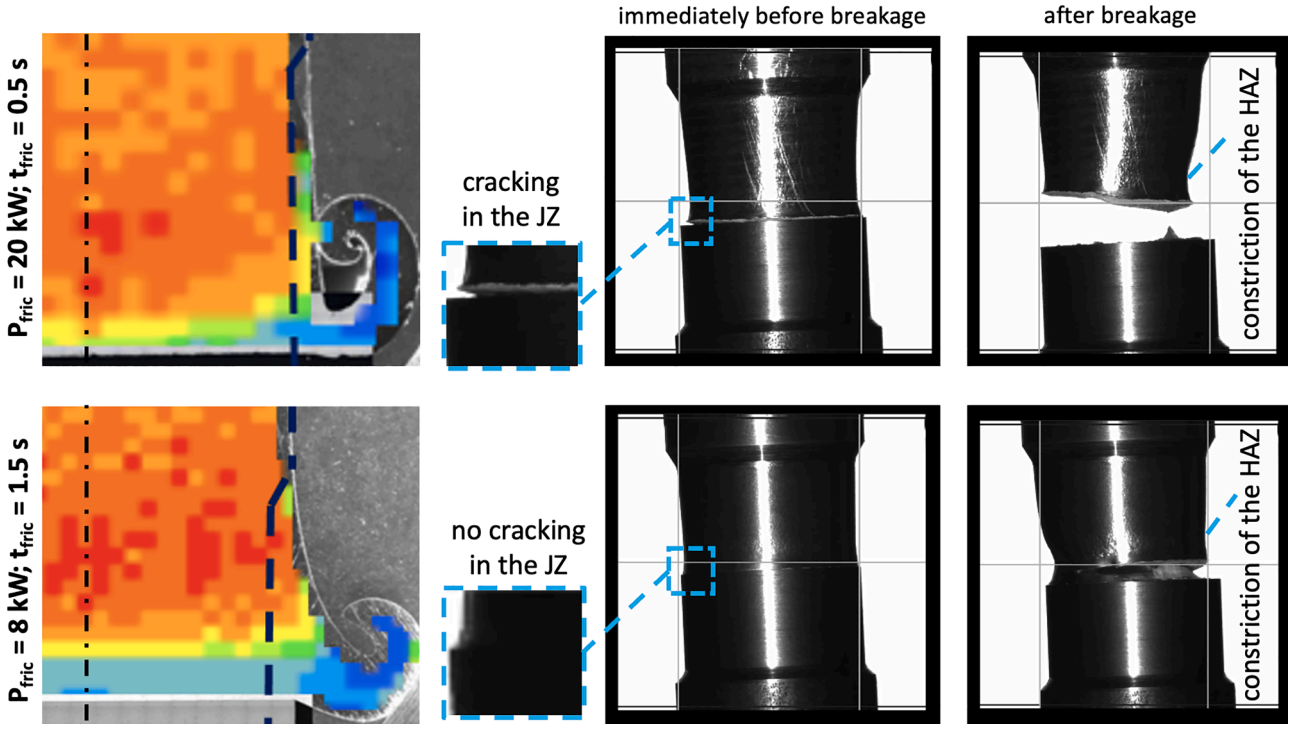

Fig. 22. Influence of the HAZ on the failure behavior in the tensile test.

It can therefore be assumed that the academically established assumption of an indirectly proportional relationship between material ductility in the joining zone and friction time, as described for example in Tashkandi and Mohamed (2020), is not generally valid, but is only applicable for identical friction power.

Metallurgy

Furthermore, the established understanding of the failure mechanism of friction welded aluminum-steel joints, as described in Gotawala and Shrivastava (2021), Ma et al. (2021), can be extended to the principle model shown in Fig. 25.

Fig. 26 shows the microscopic analysis of the three crack formation areas with moderate and intensive power welding.

It can be seen that a longer friction time not only leads to a more even heating of the aluminum material, but also distributes it to a greater extent on the steel joining surface. Dense areas of ductile aluminum residue can be seen in both the crack formation and crack propagation regions. Due to the low flow resistance in the outer radial area, preferably only the elevations of the rotational depths are covered, which leads to a fracture surface morphology corresponding to the surface structure and promotes the cracking of this area. Therefore, covering as much of this area as possible is particularly relevant for the joint strength. The increased occurrence of indicators of ductile material behavior continues in the residual fracture fragments. These are much more pronounced in the case of low frictional power and have a consistently cellular, ductile structure. In contrast, fracture surfaces that have been intensively welded for a short time exhibit smaller residual fractures which, in addition to the ductile structures, contain portions of brittle forced fractures.

According to Wan and Huang (2018), Ambroziak et al. (2014), Ochi et al. (1997), the formation of intermetallic structures in the joining zone

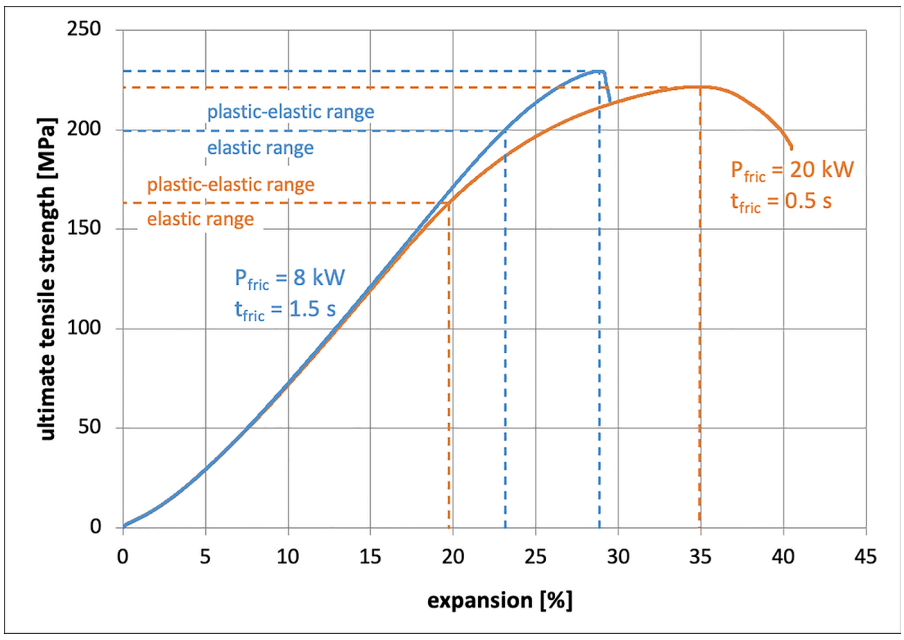

Fig. 23. Stress strain diagram of the tensile tests from Fig. 22.

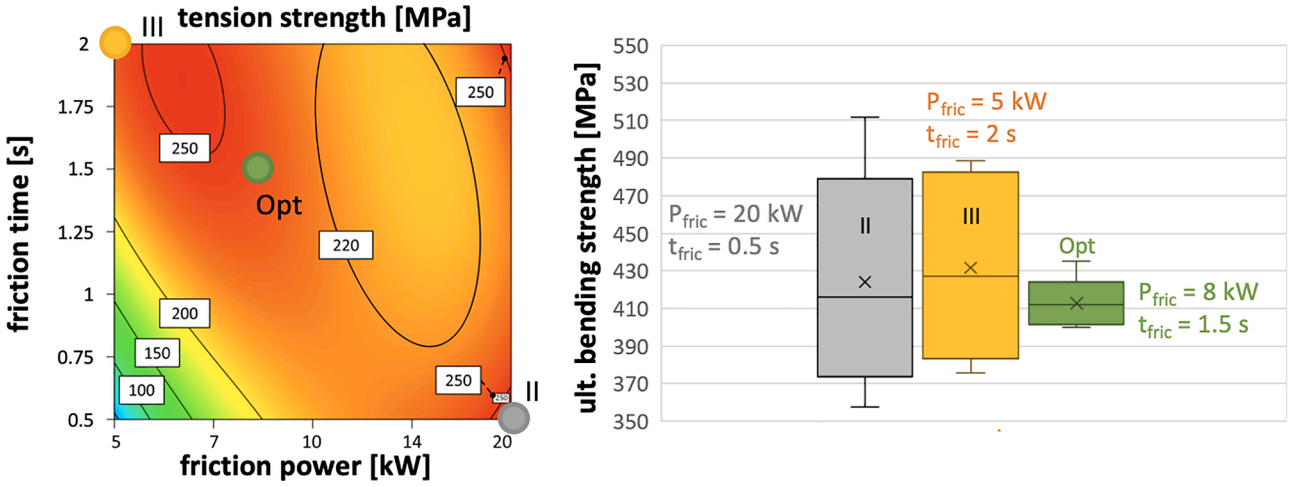

Fig. 24. Comparison of achieved bending strengths of different friction power and time levels.

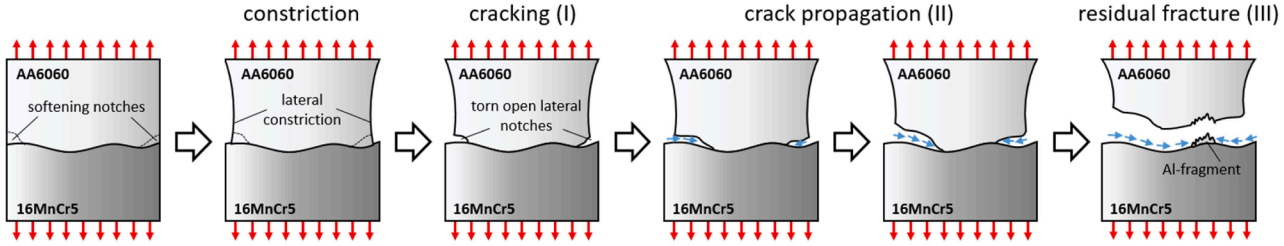

Fig. 25. Failure principle of friction welded aluminum-steel joints in the tensile test [cf. Ma et al., 2021].

is unavoidable, as there is no solubility of both elements in a solid phase in the Al-Fe system. Because these structures are considerably harder and more brittle than the base material, they can cause a degradation of the joining zone (Atabaki et al., 2014; Springer et al., 2011; Haidara et al., 2012) and must be limited in their development (Li et al., 2014; Winiczenko et al., 2017). According to [cf. Winiczenko 2016], a low temperature/degree of deformation ratio, as is the case with the specimen analysed in Fig. 26, contributes to this limitation [as there is a proportionality between phase growth and joining temperature (Wan and Huang, 2018; Kimura et al., 2017; Herbst et al., 2017; Taban et al., 2010; Reddy et al., 2008; Shinoda et al., 2001; Fukumoto et al., 1999; Fukumoto et al., 2002; Gan et al., 2017; Ikeuchi et al., 2009; Ashfaq et al., 2013; Kimura et al., 2016; Sahin et al., 1996; Yılmaz et al., 2002) and a strong material flow leads to a displacement of intermetallic

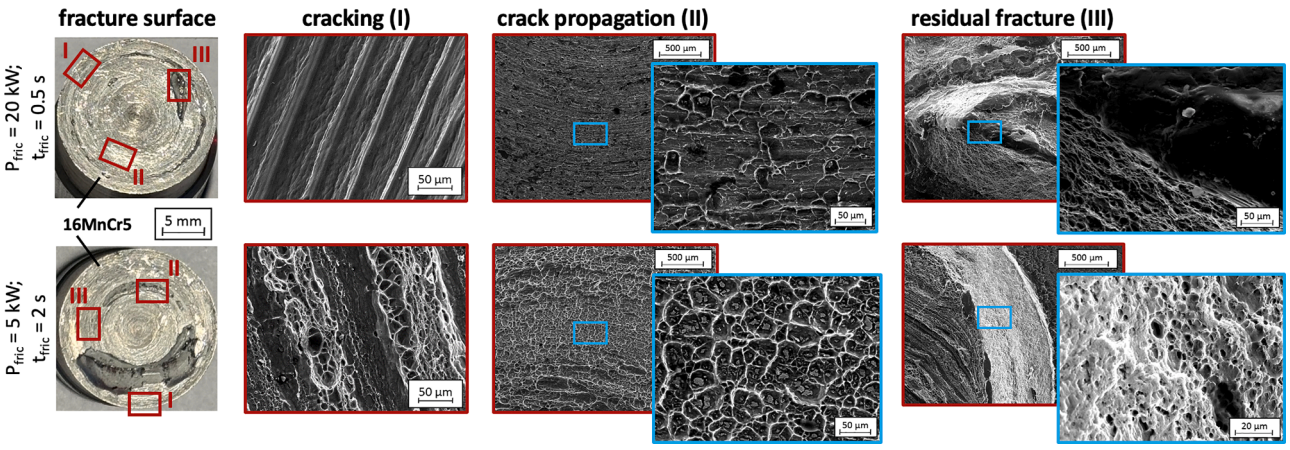

Fig. 26. Fracture surface analysis of the steel specimen.

segments]. Congruent to this, intermetallic microstructures within the two specimen cross-sections can only be detected in the lateral outer area, but not in the tensile test-relevant area. It is clear that due to the lower joining temperature at moderate friction power, only a rudimentary formation of intermetallic phases occurs despite the long exposure time. At high friction power, small phase segments are formed completely. The previously mentioned dependence of phase growth on the joining temperature is thus confirmed.

As no intermetallic phases can be detected within the areas relevant for the tensile tests, the previously presented experimental results are attributed solely to the thermal-mechanical influence on the aluminum material as explained (Fig. 27).

Discussion

A decoupling of the two process stages was achieved by the energetic consideration of the rotary friction welding process carried out in the second iteration. A response surface of the frictional power was generated from the screening data for the design of the experimental array. According to the ANOVA, the friction power depends on the rotational friction speed and the friction pressure, as expected. However, in the case of excessive rotational friction speed, insufficient dimensioning of the friction pressure can cause heat build-up. The effect of the rotational friction speed on the braking time must also be considered in this context. Particularly in the case of large friction welding machines with high inertia, a high rotational speed can lead to an unwanted, significant extension of the friction stage. This falsification of the process analysis can be avoided on a system-specific basis using the modified system model presented. Due to the decisive influence of the friction pressure on the friction time or the friction distance, large amounts of energy can only be induced at a low friction pressure level. Experimental fields for the energetic analysis of friction welding processes must therefore always be designed with these framework conditions in mind.

Based on the energetic analysis of the process, it becomes clear that a high friction energy input, due to a strong correlation with the joint quality, tends to lead to a higher joint strength, but can result in a significant overall shortening. In addition to the amount of energy input, the frictional power also has a formative effect on the thermal conditions within the joining zone and the overall course of the process. The experimental results show that a moderately intensive, longer frictioning stage can enable the induction of a higher amount of energy and the achieve a better joint strength. The reason for this is attributed to a

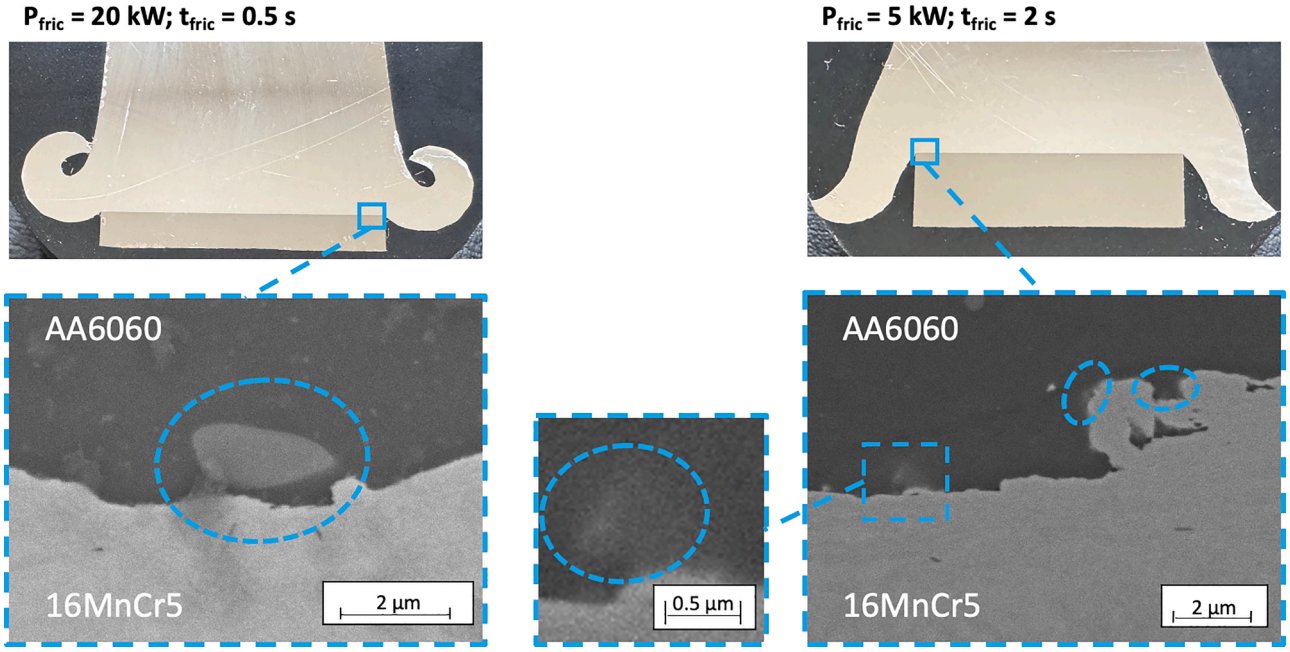

Fig. 27. Formation of intermetallic phases in the lateral outer area of the weld specimens at high (left) and moderate (right) friction power.

modification of the aluminum alloy's flow behavior. As a result of uniform heating, slow sliding of the alumi-num sample causes a shift of the maximum local deformation from the sample center to the radially outer area. As a result of shear effects, the aluminum is therefore strengthened in the edge area of the steel sample. It also reduces and equalises the amount of deformation in the radial direction. The hardening notches typical of the process, which act as weak points in the event of mechanical loads, are consequently eliminated. The experimental results also show that an intensive energy input increases the average prevailing joining temperature and thus also forces the development of the heat affected zone, which reduces the tensile strength of the joint. An optimum parameter setting prevents this and can therefore improve both the strength and the ductility of the joint zone compared to the current industrial standard. The analysis of the fracture surface shows that the latter is positively influenced by a much denser material application in the course of a longer welding time with uniform heating of the specimen.

In conclusion, moderate long term energy input is therefore identified as a promising approach for higher joint strength with good process stability and could potentially be advantageous in terms of industrial applications, both procedurally and economically.

Resume

The series of experiments carried out confirm the suitability of statistically based test methods in the context of the friction welding process. In accordance with the results of the source research, they emphasize the complex dependence of the connection quality on the process parameters. The main results of the experiments are as follows:

- An energetic approach allows the systematic decoupling of existing, cross-stage interactions between setting parameters of the frictioning and forging stage.
- Furthermore, the influence of the braking time is eliminated by this consideration.
- The prerequisite is an experimental determination of the friction power behavior in the experimental field under consideration.
- This saves experimental effort, facilitates experimental field ascent and makes interpreting the results easier.
- There is a high correlation between energy input and joint strength.
- High energy quantities can only be induced at a low friction pressure level.
- The induction intensity-time ratio influences the temperature field and thus also the material flow, the bonding and the ductility of the thermally softened zone. The characteristics of the thermally softened zone (especially in the lateral area) influence both the joint strength and the ductility of the material in the joining zone.
- Especially their condition in the lateral area is decisive for the formation of cracks.

Outlook

After the influence of the frictioning stage parameters has been methodically systematized in such a way that a decoupling between frictioning and forging stage is possible, the influence of the forging stage design on the produced joint quality is to be investigated in further experiments. It is known from the literature that the forge pressure in particular has a significant influence on the joint strength (Winkler et al., 2023a; Fuji, 2004; Kimura et al., 2017, 2005, 2009, 2011, 2023; Abdulla et al., 2018; Senthil Murugan et al., 2020; Irawan et al., 2017; Ambroziak, 2011; Fuji et al., 2001). The OFAT results shown in Fig. 28 illustrate that the effect of forge pressure diverges at different friction power levels.

The hardness curves shown in Fig. 28 suggest that this is due to the different characteristics of the HAZ. In the case of a strong characteristic, as is the case with moderate energy input, much greater forging is required to achieve a high joint strength.

Using the methodology presented in this publication, such phenomena can be identified and researched with a manageable amount of testing. The end result should be a complete, systematic investigation of the friction welding process, which forms the basis for high-quality material joints and can be reliably monitored using modern SPC applications (Fig. 29).

Contact information

Research Group of Friction Welding
University for Applied Science
Magdeburg-Stendal
Department of Engineering Sciences
and Industrial Design (IWID)
Institute of Mechanical Engineering
Breitscheidstraße 2
39114 Magdeburg, Germany
E-Mail: friction-welding@iwid.h2.de

Sampro GmbH
Dillweg 17b
39110 Magdeburg, Germany
E-Mail: info@sampro-software.com

Institute of Materials and Joining Technology
Otto-von-Guericke-University
Magdeburg
Faculty of Mechanical Engineering
Universitätsplatz 2
39106 Magdeburg, Germany
E-Mail: iwf@ovgu.de

Declaration of autonomy

The experiments, data and results presented in this publication were all carried out or generated by the University of Applied Sciences Magdeburg-Stendal and Sampro GmbH in accordance with the

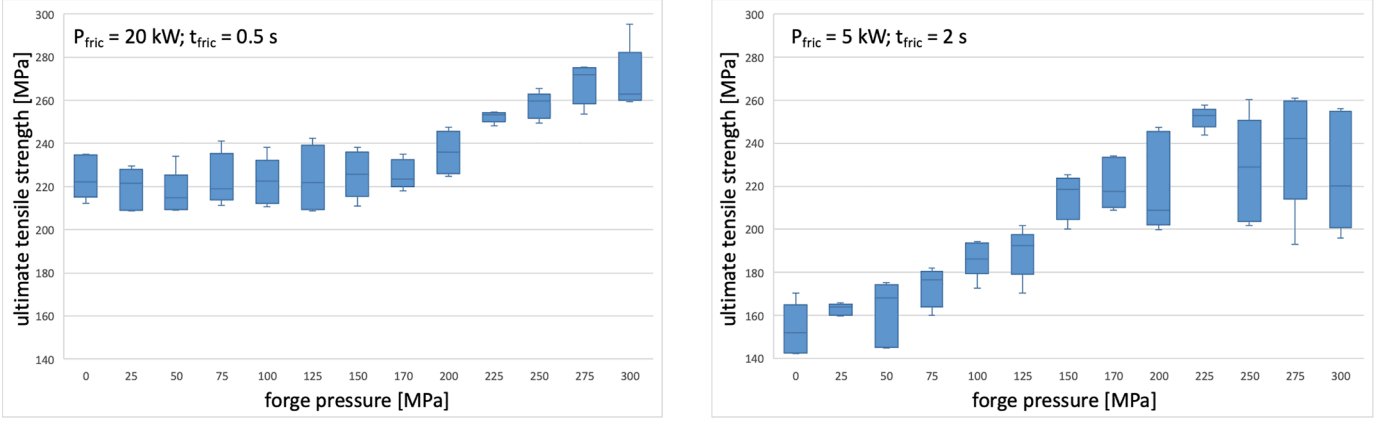

Fig. 28. OFAT of the forge pressure at intensive (left) and moderate (right) friction power.

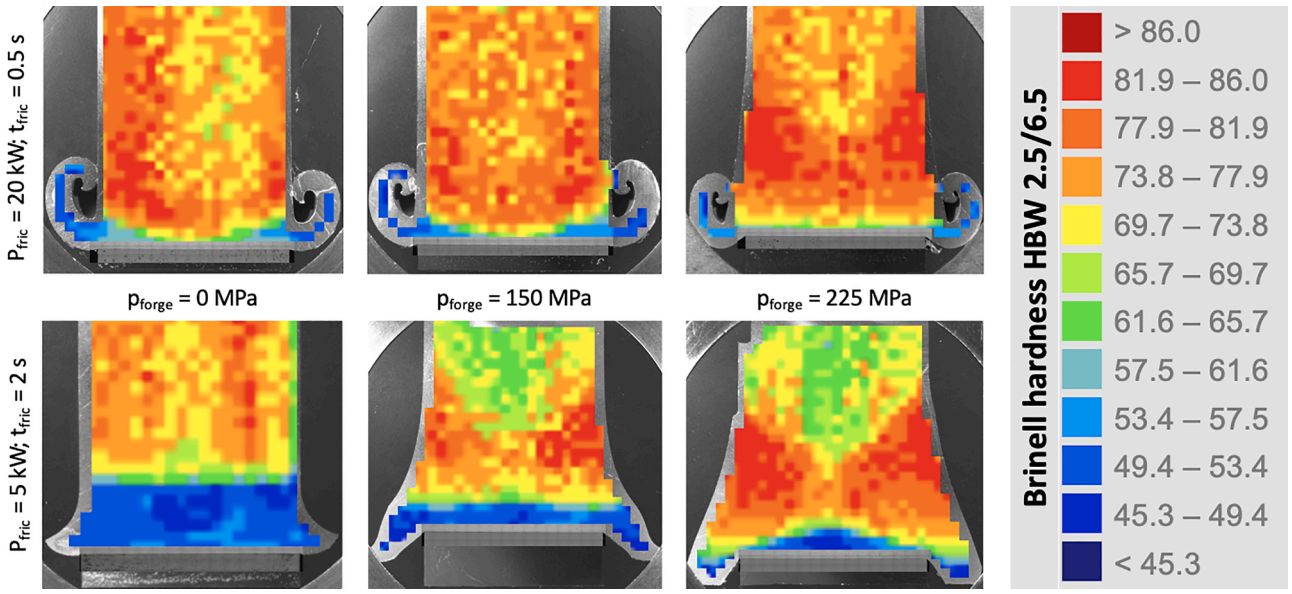

Fig. 29. Hardness gradients of the aluminum sample at different forge pressures and friction power levels.

contribution shares shown below. Third-party copyrights are of an exclusively intellectual nature and have been identified by indicating the source.

Disclosure of AI application

The authors declare that no AI-supported software was used in the course of preparing this publication.

Exclusion of conflicts of interest

There were no conflicts of interest in the course of the documented research. In this sense, the authors declare that neither financial interests nor personal relationships existed or exist that could give rise to suspicion of having influenced the work on this publication.

CRediT authorship contribution statement

M. Winkler: Writing – original draft, Visualization, Validation, Supervision, Resources, Methodology, Investigation, Funding acquisition, Formal analysis, Data curation, Conceptualization. **C. Rößler:** Writing – review & editing, Visualization, Validation, Software, Data curation. **N. Harriehausen:** Visualization, Validation, Software, Data curation. **S. Jüttner:** Writing – review & editing, Supervision. **D. Schmicker:** Writing – review & editing. **F. Trommer:** Writing – review & editing, Supervision, Project administration, Funding acquisition.

Declaration of competing interest

The authors declare that they have no known competing financial interests or personal relationships that could have appeared to influence the work reported in this paper.

Data availability

Data will be made available on request.

Acknowledgment

The research data of the parameter screening were generated as part of the joint project "Hybrid lightweight construction of solid components using friction welded aluminum-steel and aluminum-cast iron joints (HyLight)". This was funded by the "Lightweight Construction" technology transfer program of the Federal Ministry of Economics and Climate Protection (BMWK) - administered by the Project Funder Jülich (PTJ). The authors would like to thank the sponsors of the project.

Further thanks are due to Prof. Dr. J.-G. Swanson for the linguistic review of the paper.

Supported by:
Federal Ministry for Economic Affairs and Climate Action
on the basis of a decision by the German Bundestag

References

Abdulla, F.A.M., Irawan, Y.S., Darmadi, D.B., 2018. Tensile strength and macro-microstructures of A6061 CDFW weld joint influenced by pressure and holding time in the upset stage. J. Rekayasa Mesin 9 (2), 149–154.

Adalarasan, R., Santhanakumar, M., Shanmuga Sundaram, A., 2014. Optimization of weld characteristics of friction welded AA 6061-AA 6351 joints using grey-principal component analysis (G-PCA). J. Mech. Sci. Technol. 28, 301–307.

Adin, M.Ş., İşcan, B., Baday, Ş., 2022. Optimization of welding parameters of AISI 431 and AISI 1020 joints joined by friction welding using taguchi method. Bilecik Şeyh Edebali Üniv. Bilim. Derg. 9 (1), 453–470.

Ajith, P., et al., 2015. Multiobjective optimization of friction welding of UNS S32205 duplex stainless steel. Def. Technol. 11 (2), 157–165.

Alves, E.P., Neto, F.P., An, C.Y., 2010. Welding of AA1050 aluminum with AISI 304 stainless steel by rotary friction welding process. J. Aerosp. Technol. Manag. 2, 301–306.

Ambroziak, A., 1999. Selection of transition layers for dissimilar friction-welded joints [\Polish original title: Dobór warstw przejściowych dla różnoimiennych złączy zgrzewanych tarciowo]. Bulletin of the Institute of Welding in Gliwice 43 (5), 55–58.

Ambroziak, A., 2011. Friction welding of materials with different properties [\Polish original title: Zgrzewanie Tarciowe Materiałow o Roznych Właściwosciach]. In: Publisher of Wroclaw University of Technology, Wroclaw.

Ambroziak, A., et al., 2014. Friction welding of aluminium and aluminium alloys with steel. Adv. Mater. Sci. Eng. 1, 15. https://doi.org/10.1155/2014/981653.

Anand, K., et al., 2015b. A comparative study of artificial neural network and response surface methodology for optimization of friction welding of Incoloy 800 H. Acta Metal. Sin. 28, 892–902 (English Letters).

Anand, K., et al., 2015a. Artificial neural network modeling studies to predict the friction welding process parameters of Incoloy 800H joints. Eng. Sci. Technol. Int. J. 18 (3), 394–407.

Ananthapadmanaban, D., et al., 2009. A study of mechanical properties of friction welded mild steel to stainless steel joints. Mater. Des. 30 (7), 2642–2646.
Ashfaq, M., et al., 2013. Improving strength of stainless steel/aluminum alloy friction welds by modifying faying surface design. J. Mater. Eng. Perform. 22, 376–383.
Ashfaqa, M., et al., 2011. Friction welding of titanium to 304L stainless steel using interlayers. Reibschweißen von Titan an rostfreiem Stahl 304L unter Anwendung von Zwischenschichten Prakt. Metallogr. 48, 4.
Asif, M.M., Shrikrishna, K.A., Sathiya, P., 2016. Optimization of process parameters of friction welding of UNS S31803 duplex stainless steels joints. Adv. Manuf. 4, 55–65.
Atabaki, M.M., et al., 2014. Welding of aluminum alloys to steels: an overview. J. Manuf. Sci. Prod. 14 (2), 59–78.
Bakkiyaraj, M., et al., 2022. Influence of process parameters on tensile strength of the friction welded aa6063-T6 joints by box–behnken design approach. Adv. Mater. Sci. Eng. 1, 11. https://onlinelibrary.wiley.com/doi/pdf/10.1155/2022/3463726.
Balalan, Z., et al., 2015. Functional ANOVA investigation of the effects of friction welding parameters on the joint characteristics of aluminum based MMC to AISI 304 stainless steel. Mater. Test. 57 (6), 558–566.
Bendzsak, G., North, T., Li, Z., 1997. Numerical model for steady-state flow in friction welding. Acta Mater. 45 (4), 1735–1745.
Bouche, K., Barbier, F., Coulet, A., 1998. Intermetallic compound layer growth between solid iron and molten aluminium. Mater. Sci. Eng. A 249 (1–2), 167–175.
Cheepu, M., Che, W.S., 2019. Characterization of microstructure and interface reactions in friction welded bimetallic joints of titanium to 304 stainless steel using nickel interlayer. Trans. Indian Inst. Met. 72 (6), 1597–1601.
Draugelates, U., Schram, A., Kettler, C., 2000. Friction welding of magnesium alloys - Lightweight construction concepts with magnesium materials call for appropriate joining techniques (\German original title: reibschweissen von Magnesiumlegierungen - Leichtbaukonzepte mit Magnesiumwerkstoffen rufen nach entsprechenden Fügetechniken). J. Manuf. Technol. Autom. 49 (12), 56–61 (\Fachzeitschrift für die Fertigungstechnik und Automation).
Fan, Z., et al., 2015. Experimental investigation on fabrication of Al/Fe bi-metal tubes by the magnetic pulse cladding process. Int. J. Adv. Manuf. Technol. 83 (5–8), 1409–1418.
Fan, Z., et al., 2016. Experimental investigation on fabrication of Al/Fe bi-metal tubes by the magnetic pulse cladding process. Int. J. Adv. Manuf. Technol. 83 (5–8), 1409–1418.
Fuhaid, M.S., et al., 2020. Manufacturing and friction welding of aluminium matrix composites–review of current status and future directions. Test Eng. Manag. 1122–1130.
Fuji, A., et al., 2001. Properties of as welded and heat treated pure titanium–7075 Al–Zn–Mg alloy friction weld joints. Sci. Technol. Weld. Join. 6 (1), 23–30.
Fuji, A., 2004. Friction welding of Al–Mg–Si alloy to Ni–Cr–Mo low alloy steel. Sci. Technol. Weld. Join. 9 (1), 83–89.
Fukumoto, S., et al., 1999. Friction welding process of 5052 aluminium alloy to 304 stainless steel. Mater. Sci. Technol. 15 (9), 1080–1086.
Fukumoto, S., et al., 2002. Formation process of reaction layer between aluminium alloys and stainless steel by friction welding. Weld. Int. 16 (12), 941–946.
Gan, W.M., et al., 2017. Microstructure and residual stress in rotary friction welded dissimilar metals of AA7020 aluminium alloy with 316L steel. Mater. Sci. Forum 879, 572–577.
German Institute for Standardization (DIN), 2000. Metallic Materials - Bending Test. Beuth Verlag, Berlin, p. 20.
German Institute for Standardization (DIN), 2005. Aluminum and Aluminum Alloys-Chemical Composition and Form of Semi-Finished Products-Part 3: Chemical Composition and Product Forms. Beuth-Verlag, Berlin, p. 38.
German Institute for Standardization (DIN), 2020. Metallic Materials - Tensile Test - Part 1: Test Method At Room Temperature. Beuth-Verlag, Berlin, p. 96.
German Institute for Standardization (DIN), 2022. Steels Intended For Heat Treatment, Alloy Steels and Free-Cutting Steels - Part 3: Case-Hardening Steels. Beuth-Verlag, Berlin, p. 43.
German Welding Society (DVS), 2009. Rotary friction welding: process, terms, materials. Friction Welding of Metal Materials. Beuth-Verlag, Berlin, p. 7.
German Welding Society (DVS), 2011. Characteristics and production of the joint and monitoring of the welding process. Friction Welding of Metal Materials. Beuth-Verlag, Berlin, p. 7.
Ghari, H., et al., 2024. Metallurgical characteristics of aluminum-steel joints manufactured by rotary friction welding: a review and statistical analysis. J. Mater. Res. Technol. 30, 2520–2550.
Gomeringer, R., et al., 2020. Metal Table Book [\German Original title: Tabellenbuch Metall]. Verlag Europa Lehrmittel Nourney, Vollmer GmbH & Company KG.
Gotawala, N., Shrivastava, A., 2021. Investigation of interface microstructure and mechanical properties of rotatory friction welded dissimilar aluminum-steel joints. Mater. Sci. Eng. A 825, 141900.
Gottstein, G., 2007. Physical Basics of Materials Science [\German Original title: Physikalische Grundlagen Der Materialkunde], 3. Springer-Verlag, p. 520.
Grant, B., et al., 2009. Finite element process modelling of inertia friction welding advanced nickel-based superalloy. Mater. Sci. Eng. A 513, 366–375.
Haidara, F., et al., 2012. Phase formation in Al–Fe thin film systems. Intermetallics 23, 143–147 (Barking).
Herbst, S., et al., 2017. Microstructure and mechanical properties of friction welded steel-aluminum hybrid components after T6 heat treatment. Mater. Sci. Eng. A 696, 33–41.
Hincapié, O.D., et al., 2020. Weldability of aluminum-steel joints using continuous drive friction welding process, without the presence of intermetallic compounds. Eng. J. 24 (1), 129–144.
Ihsan, K., et al., 2013. Optimization of tensile strength of friction welded AISI 1040 and AISI 304L steels according to statistics analysis (ANOVA). Mater. Test. 55 (6), 435–441.
Ikeuchi, K., et al., 2005. Effect of interfacial reaction layer on bond strength of friction-bonded joint of Al alloys to steel. Trans. JWRI 34 (1), 10.
Ikeuchi, K., et al., 2009. Effects of carbon content on intermetallic compound layer and joint strength in friction welding of Al alloy to steel. Weld. World 53, R135–R139.
Irawan, Y.S., Suprapto, W., Oerbandono, T., 2017. Torsion strength of round bar A6061 friction weld joint influenced by friction time, upset force and one-side cone geometry. J. Environ. Eng. Sustain. Technol. 4 (2), 78–84.
Jank, N., Staufer, H., Bruckner, J., 2008. Welded joints of steel with aluminum - a perspective for the future [\German original title: Schweißverbindungen von stahl mit aluminium – eine perspektive für die zukunft]. BHM B. Hüttenmänn. Monatsh. 5 (153), 189–192.
Kawai, G., et al., 2000. Friction weldability of aluminium alloys to carbon steel. Weld. Int. 14 (2), 101–107.
Kes, P.H., 1989. Contribution to Friction Welding of Ductile Cast Iron Materials [\German original title: Beitrag zum Reibschweißen duktiler Eisengusswerkstoffe]. RWTH Aachen, Düsseldorf.
Khalfallah, F., et al., 2020. Optimization by RSM on rotary friction welding of AA1100 aluminum alloy and mild steel. Int. Rev. Appl. Sci. Eng. 11 (1), 34–42.
Kimura, M., et al., 2005. Effect of friction welding conditions and aging treatment on mechanical properties of A7075-T6 aluminium alloy friction joints. Sci. Technol. Weld. Join. 10 (4), 406–412.
Kimura, M., et al., 2009. Joining phenomena and joint strength of friction welded joint between aluminium–magnesium alloy (AA5052) and low carbon steel. Sci. Technol. Weld. Join. 14 (7), 655–661.
Kimura, M., et al., 2011. Effect of friction welding condition and weld faying surface properties on tensile strength of friction welded joint between pure titanium and pure copper. J. Solid Mech. Mater. Eng. 5 (12), 849–865.
Kimura, M., et al., 2016. Friction welding technique and joint properties of thin-walled pipe friction-welded joint between type 6063 aluminum alloy and AISI 304 austenitic stainless steel. Int. J. Adv. Manuf. Technol. 82 (1–4), 489–499.
Kimura, M., et al., 2017. Effect of friction welding condition on joining phenomena and mechanical properties of friction welded joint between 6063 aluminium alloy and AISI 304 stainless steel. J. Manuf. Process. 26, 178–187.
Kimura, M., et al., 2023. Improving the tensile strength between pure Al and low carbon steel joint fabricated by friction welding. J. Mater. Eng. Perform. 32 (10), 4655–4667.
Kumar, G.S., Ramakrishnan, R., 2020. Influence of mechanical characteristics of friction welded ferrite stainless steel joint through novel mathematical model using buckingham's pi theorem. Int. J. Mech. Prod. Eng. Res. Dev. 10 (1), 185–198.
Li, P., et al., 2014. Effect of friction time on mechanical and metallurgical properties of continuous drive friction welded Ti6Al4V/SUS321 joints. Mater. Des. 56, 649–656 (1980-2015).
Li, Q., et al., 2006. Finite element simulation of deformation behavior in friction welding of Al-Cu-Mg alloy. J. Mater. Eng. Perform. 15, 627–631.
Liu, Y., et al., 2020. Microstructure and tensile strength of aluminum/stainless steel joint welded by inertia friction and continuous drive friction. Weld. World 64, 1799–1809.
Lotz, M., 2013. Increasing the Manufacturing Accuracy of Flywheel Friction Welding using Model-Based Control Methods, 271. Herbert Utz Verlag [\German Original title: Increasing the Manufacturing Accuracy of Flywheel Friction Welding Using Model-Based Control Methods].
Ma, H., et al., 2021. Interfacial microstructure and property of 6061 aluminium alloy/stainless steel hybrid inertia friction welded joint with different steel surface roughness. Mater. Charact. 179, 111347.
Maalekian, M., 2007. Friction welding–critical assessment of literature. Sci. Technol. Weld. Join. 12 (8), 738–759.
Mehta, K.P., 2019. A review on friction-based joining of dissimilar aluminum–steel joints. J. Mater. Res. 34 (1), 78–96.
Murugan, S.S., Sathiya, P., 2023. A review of friction welding research to address the influence, development, similar & dissimilar welding. Ann. Dunarea de Jos Univ. Galati Fascicle XII Weld. Equip. Technol. 34, 65–88.
Ochi, H., et al., 1993. Friction welding of titanium and SUS304 stainless steel. J. Jpn. Inst. Light Met. 43 (7), 365–371.
Ochi, H., et al., 1997. Friction welding of aluminum alloy and steel. In: Proceedings of the Seventh International Offshore and Polar Engineering Conference. OnePetro.
Oosterkamp, A., Djapic, L., Nordeide, A., 2004. Kissing bond'phenomena in solid-state welds of aluminum alloys. Weld. J. 83 (8), 225. New Yorkff.
Ostermann, F., 2015. Aluminum Application Technology [\German Original title: Anwendungstechnologie Aluminium], 3. VDI-Book, Berlin/Heidelberg.
Pachal, A.S., Bagesar, A., 2013. Taguchi optimization of process parameters in friction welding of 6061 aluminum alloy and 304 steel: a review. Int. J. Emerg. Technol. Adv. Eng 3, 229–233.
Paventhan, R., et al., 2023. Optimizing friction welding parameters in AISI 304 austenitic stainless steel and commercial copper dissimilar joints. Coatings 13 (2), 261 ff.
Paventhan, R., Lakshminarayanan, P., Balasubramanian, V., 2011. Prediction and optimization of friction welding parameters for joining aluminium alloy and stainless steel. Trans. Nonferrous Met. Soc. China 21 (7), 1480–1485.
Paventhan, R., Lakshminarayanan, P., Balasubramanian, V., 2012. Optimization of friction welding process parameters for joining carbon steel and stainless steel. J. Iron Steel Res. Int. 19 (1), 66–71.
Pohle, C., 1999. Welding of material combinations [\German original title: Schweißen von Werkstoffkombinationen], Vol. 140. DVS Media.

Prokopczuk, P., 2011. New Manufacturing Processes for Integrally Bladed Rotors [\German original title: Neue Herstellungsverfahren Für Integral Beschaufelte Rotoren]. Technical University Munich.
Rafi, H.K., et al., 2010. Microstructure and tensile properties of friction welded aluminum alloy AA7075-T6. Mater. Des. 31 (5), 2375–2380.
Rajamani, G., Shunmugam, M., Rao, K., 1992. Parameter optimization and properties of friction welded quenched and tempered steel. Weld. J. 71, 225. New Yorkff.
Rangasamy, S., et al., 2023. Optimization of mechanical properties of rotary friction welding parameters of low alloy steel tubes using design of experiments concept. Int. J. Interact. Des. Manuf. IJIDeM 1–15.
Reddy, M.G., Rao, S.A., Mohandas, T., 2008. Role of electroplated interlayer in continuous drive friction welding of AA6061 to AISI 304 dissimilar metals. Sci. Technol. Weld. Join. 13 (7), 619–628.
Reiners, G., Kreye, H., 1988. Mikrostruktur und mechanische eigenschaften von reibschweissverbindungen aus aluminium und stahl. Schweiß. Schneid. 40 (123), 9.
Rößler, C., 2023. Numerical Assessment of the Residual Stress Formation in Rotary Friction Welding. Otto-von-Guericke-Universität, Magdeburg, p. 99. Fakultät Für Maschinenbau.
Ruge, J., 2013. Handbook of Welding Technology: Volume II: Processes and Manufacturing [\German original title: Handbuch der Schweißtechnik: Band II: Verfahren und Fertigung], Vol. 3. Springer-Verlag.
Sahin, A., Yilbas, B., Al-Garni, A., 1996. Friction welding of Al-Al, Al-steel, and steel-steel samples. J. Mater. Eng. Perform. 5, 89–99.
Sahin, M., 2009. Joining of stainless-steel and aluminium materials by friction welding. Int. J. Adv. Manuf. Technol. 41, 487–497.
Sasmito, A., Ilman, M.N., Iswanto, P.T., 2023. Effects of rotational speed on the mechanical properties and performance of AA6061-T6 aluminium alloy in similar rotary friction welding. Weld. Int. 37 (9), 519–530.
Sathiya, P., Aravindan, S., Haq, A.N., & Panneerselvam, K., Optimization of friction welding parameters using simulated annealing. 2006. Indian J. Eng. Mater. Scie. 13 (1), 37-44.
Sathiya, P., et al., 2009. Optimization of friction welding parameters using evolutionary computational techniques. J. Mater. Process. Technol. 209 (5), 2576–2584.
Sathiya, P., Aravindan, S., Haq, A.N., 2004. Friction welding of austenitic stainless steel and optimization of weld quality. In: Proceedings of the International Symposium of Research Students on Materials Science and Engineering.
Sathiya, P., Aravindan, S., Noorul Haq, A., 2006b. Optimization for friction welding parameters with multiple performance characteristics. Int. J. Mech. Mater. Des. 3, 309–318.
Satyanarayana, V., Reddy, G.M., Mohandas, T., 2005. Dissimilar metal friction welding of austenitic–ferritic stainless steels. J. Mater. Process. Technol. 160 (2), 128–137.
Schmicker, D., 2015. A Holistic Approach on the Simulation of Rotary Friction Welding. Otto-von-Guericke Universität Magdeburg, Berlin. Fakultät für Maschinenbau.
Seli, H., et al., 2010. Mechanical evaluation and thermal modelling of friction welding of mild steel and aluminium. J. Mater. Process. Technol. 210 (9), 1209–1216.
Selvamani, S., Divagar, S., Vigneshwar, M., 2015. Application of response surface methodology (RSM) in friction welding AISI 1020 grade steel joints. Int. J. Eng. Res. Afr. 16, 38–44.
Selvaraj, R., et al., 2023. Optimization of process parameters of rotary friction welding of low alloy steel tubes using response surface methodology. Forces Mech. 10, 20, 100175.
Senthil Murugan, S., Sathiya, P., Noorul Haq, A., 2020. Experimental study on the effect of silver, nickel and chromium interlayers and upset pressure in joining SS304L-AA6063 alloys through direct drive friction welding process. J. Braz. Soc. Mech. Sci. Eng. 42, 1–17.
Shanjeevi, C., Kumar, S.S., Sathiya, P., 2016. Multi-objective optimization of friction welding parameters in AISI 304L austenitic stainless steel and copper joints. Proc. Inst. Mech. Eng. Part B J. Eng. Manuf. 230 (3), 449–457.
Shinoda, T., et al., 2001. Friction welding of aluminium and plain low carbon steel. Weld. Int. 15 (6), 438–445.
Springer, H., et al., 2011. On the formation and growth of intermetallic phases during interdiffusion between low-carbon steel and aluminum alloys. Acta Mater. 59 (4), 1586–1600.
Sreenivasan, K., Kumar, S.S., Katiravan, J., 2019. Genetic algorithm based optimization of friction welding process parameters on AA7075-SiC composite. Eng. Sci. Technol. Int. J. 22 (4), 1136–1148.
Stalin, B., et al., 2020. Friction welding parametric optimization of AISI 310L austenitic stainless steel weld joints-Grey relational investigation. AIP Conf. Proc. 2283 (020141), 8. AIP Publishing LLC.
Sun, G.Q., et al., 2019. Welding parameter selection and short fatigue crack growth of dissimilar aluminum alloy friction stir welded joint. Weld. World 63 (6), 1761–1769.
Taban, E., Gould, J.E., Lippold, J.C., 2010. Dissimilar friction welding of 6061-T6 aluminum and AISI 1018 steel: properties and microstructural characterization. Mater. Des. 31 (5), 2305–2311 (1980-2015).
Tasdemir, C., 2020. Investigations Into the Joining of Aluminum Gravity Die Castings Using Friction Flywheel Welding [\German original title: Untersuchungen zum Fügen von Aluminium-Kokillenguss mittels Schwungradreibschweißen]. Aachen University of Technology, Aachen, p. 215. Department of Materials Science and Engineering.
Tashkandi, M.A., Mohamed, M.I., 2020. Effect of friction time on the mechanical and microstructural properties of AA6061 joints by continuous drive friction welding. Eng. Technol. Appl. Sci. Res. 10 (3), 5596–5602.
Trommer, F., Investigations into orbital Friction Welding for selected Metal Materials [\German original title: untersuchungen zum Orbitalreibschweißen für ausgewählte Metallwerkstoffe], in Institute For Materials and Joining Technology (IWF). 2011, Otto-von-Guericke-University: Magdeburg.
Uday, M., et al., 2010. Advances in friction welding process: a review. Sci. Technol. Weld. Join. 15 (7), 534–558.
Uzkut, M., Ünlü, B.S., Akdağ, M., 2011. Determination of optimum welding parameters in connecting high alloyed X53CrMnNiN219 and X45CrSi93 steels by friction welding. Bull. Mater. Sci. 34, 815–823.
Varjenju, O.P., Tornem, P., Dele, N., Jekla, N.B., 2016. Optimizing the parameters for friction welding stainless steel to copper parts. Mater. Tehnol. 50 (1), 109–115.
Wan, L., Huang, Y., 2018. Friction welding of AA6061 to AISI 316L steel: characteristic analysis and novel design equipment. Int. J. Adv. Manuf. Technol. 95.
Wang, L., et al., 2005. Energy-input-based finite-element process modeling of inertia welding. Metall. Mater. Trans. B 36, 513–523.
Wang, T., et al., 2018. Friction stir scribe welding technique for dissimilar joining of aluminium and galvanised steel. Sci. Technol. Weld. Join. 23 (3), 249–255.
Winiczenko, R., 2016. Effect of friction welding parameters on the tensile strength and microstructural properties of dissimilar AISI 1020-ASTM A536 joints. Int. J. Adv. Manuf. Technol. 84, 941–955.
Winiczenko, R., et al., 2017. Friction welding of tungsten heavy alloy with aluminium alloy. J. Mater. Process. Technol. 246, 42–55.
Winkler, M., et al., 2022. Investigation of the friction weldability of an AlSi10MnMg-alloy reinforced with 30 Vol.-% silicon carbide particles with the adequate monolithic material. J. Adv. Join. Process. 5, 10, 100101.
Winkler, M., 2023. Development of a Methodology for Researching and Optimizing Friction Welding Processes [\German Original title: Entwicklung einer Methodik zur Erforschung und Optimierung von Reibschweißprozessen]. Otto-von-Guericke-University Magdeburg. Faculty of Human Sciences.
Winkler, M., et al., 2023b. The investigation of friction welding processes for the production of hybrid material joints - a holistic methodical approach. In: Proceedings of the Friction Welding Symposium. Magdeburg. University for Applied Science Magdeburg-Stendal, Raiser GmbH & Sampro GmbH, pp. 191–207.
Winkler, M., Jüttner, S., Trommer, F., 2023a. The potential of friction-welded material joints in the maritime sector and their requirements for joining technology using the example of friction-welded aluminum joints. In: Proceedings of the Symposium "Steel in Hydraulic Engineering 2023″, pp. 143–163. Stahlmann, Joachim: Braunschweig.
Wysocki, J., Grabian, J., Przetakiewicz, W., 2007. Continuous drive friction welding of cast AlSi/SiC(p) metal matrix composites. Arch. Foundry Eng. 7 (1), 47–52.
Yamamoto, N., et al., 2004. Interfacial layer in friction-bonded joint of low carbon steel to Al-Mg alloy (AA5083) and its influence on bond strength. Mater. Trans. 45 (2), 296–299.
Yamamoto, N., et al., 2007. Formation of intermetallic compounds in friction bonding of Al alloys to steel. Mater. Sci. Forum 539-543, 3865–3871.
Yılmaz, M., Çöl, M., Acet, M., 2002. Interface properties of aluminum/steel friction-welded components. Mater. Charact. 49 (5), 421–429.